Acta Neuropathologica (2025) 149:8
https://doi.org/10.1007/s00401-025-02845-y

ORIGINAL PAPER

Concurrent RB1 and P53 pathway disruption predisposes to the development of a primitive neuronal component in high-grade gliomas depending on MYC-driven EBF3 transcription

Francesca Pagani[1,2] · Francesca Orzan[3,4] · Sara Lago[5] · Francesca De Bacco[3,4] · Marta Prelli[3,4] · Manuela Cominelli[1] · Elena Somenza[1,6] · Magdalena Gryzik[1,7] · Piera Balzarini[1] · Davide Ceresa[8] · Daniela Marubbi[8,9] · Claudio Isella[3,4] · Giovanni Crisafulli[10] · Maura Poli[7] · Paolo Malatesta[8,9] · Rossella Galli[11] · Roberto Ronca[6] · Alessio Zippo[5] · Carla Boccaccio[3,4] · Pietro Luigi Poliani[1,12]

Received: 21 October 2024 / Revised: 5 January 2025 / Accepted: 6 January 2025
© The Author(s), under exclusive licence to Springer-Verlag GmbH Germany, part of Springer Nature 2025

Abstract

The foremost feature of glioblastoma (GBM), the most frequent malignant brain tumours in adults, is a remarkable degree of intra- and inter-tumour heterogeneity reflecting the coexistence within the tumour bulk of different cell populations displaying distinctive genetic and transcriptomic profiles. GBM with primitive neuronal component (PNC), recently identified by DNA methylation-based classification as a peculiar GBM subtype (GBM-PNC), is a poorly recognized and aggressive GBM variant characterised by nodules containing cells with primitive neuronal differentiation along with conventional GBM areas. In addition, the presence of a PNC component has been also reported in *IDH*-mutant high-grade gliomas (HGGs), and to a lesser extent to other HGGs, suggesting that regardless from being *IDH*-mutant or *IDH*-wildtype, peculiar genetic and/or epigenetic events may contribute to the phenotypic skewing with the emergence of the PNC phenotype. However, a clear hypothesis on the mechanisms responsible for this phenotypic skewing is still lacking. We assumed that the biphasic nature of these entities represents a unique model to investigate the relationships between genetic alterations and their phenotypic manifestations. In this study we show that in HGGs with PNC features both components are highly enriched in genetic alterations directly causing cell cycle deregulation (*RB* inactivation or *CDK4* amplification) and p53 pathway inactivation (*TP53* mutations or *MDM2/4* amplification). However, the PNC component displays further upregulation of transcriptional pathways associated with proliferative activity, including overexpression of MYC target genes. Notably, the PNC phenotype relies on the expression of EBF3, an early neurogenic transcription factor, which is directly controlled by MYC transcription factors in accessible chromatin sites. Overall our findings indicate that the concomitant presence of genetic alterations, impinging on both cell cycle and p53 pathway control, strongly predisposes GBM to develop a concomitant poorly differentiated primitive phenotype depending on MYC-driven EBF3 transcription in a subset of glioma stem-like progenitor cells.

Keywords High-grade glioma · Glioblastoma · Primitive neuronal component · *RB1* · Early B-cell factor · *MYC* · Tumour heterogeneity

Introduction

Glioblastoma (GBM) is the most frequent malignant central nervous system (CNS) tumour in adults [59]. Despite multimodal therapeutic approaches, including surgery, chemotherapy and radiotherapy, prognosis remains dismal with an average survival time for patients of only 15 months and a 5-year survival rate lower than 5% [1, 77]. Genetic, epigenetic and phenotypic features of GBM have been deeply characterised. Nevertheless, assessment of innovative potential targeted therapies has been disappointing, mostly due to a remarkable degree of intra- and inter-tumour heterogeneity reflecting the coexistence within the same tumour of different cell populations displaying distinctive genetic and transcriptomic profiles [58, 85, 86, 88]. Recently, a number of studies have reported that at single cell level, GBMs are composed of a mix of different cell populations each enriched for specific genetic and epigenetic events, resulting in a combination of different lineage-restricted cellular states

Extended author information available on the last page of the article

Published online: 16 January 2025

that recapitulate neurodevelopmental pathways [6, 56, 65]. Despite these findings, the source of this complexity still remains unclear and deserves to be investigated [65]. This huge tumour heterogeneity is also evidenced by the presence of a wide spectrum of different histological entities and molecular subtypes that renders glioma classification difficult, a limitation partially overcome by DNA methylation profiling that has been shown to be highly robust and reproducible [10]. According to the 5th Edition of World Health Organization (WHO) classification of CNS tumours (CNS WHO 2021), adult-type diffuse high-grade gliomas (HGGs) are classified into two different major categories depending on the presence or absence of isocitrate dehydrogenase 1 and 2 (*IDH1* and *IDH2*) mutations [48]. GBMs are currently exclusively defined as adult-type HGGs *IDH*-wildtype and diagnosis is based on either histological features, such as mitotic activity, microvascular proliferation and/or necrosis, and the presence of specific molecular alteration, including *TERT* (Telomerase reverse transcriptase) promoter mutation, *EGFR* (Epidermal Growth Factor Receptor) gene amplification and combined gain of entire chromosome 7 and loss of entire chromosome 10 (+7/−10) [3]. On the other hand, *IDH*-mutant diffuse astrocytic tumours are considered a separate entity graded as CNS WHO grade 2, 3 or 4 depending on different histological and molecular features [3, 48]. Among the different histological entities, glioblastoma with primitive neuronal component (PNC), currently defined as GBM with PNC component (GBM-PNC) [48], represent a rare variant [14], recently identified by DNA methylation-based classification as a peculiar GBM subtype [80]. However, the presence of a PNC component have been also reported in *IDH*-mutant high-grade astrocytomas [14, 36, 74, 92] and to a lesser extent in *H3 G34*–mutant diffuse hemispheric HGGs [40] and in *H3 K27*-altered diffuse midline HGGs [73]. This observation suggests that in HGGs, regardless from being *IDH*-mutant or *IDH*-wildtype, peculiar genetic and/or epigenetic events may contribute to the phenotypic skewing of glioma stem-like cells (GSCs) precursor cells with the emergence of distinct tumour subclones, including PNC. HGGs with a PNC component consist of a biphasic tumour with a classical high grade histology associated with well demarcated nodules composed of poorly differentiated immature cells with variable neuronal differentiation, loss of GFAP expression, markedly increased cellularity, severe anaplasia and high mitotic-karyorrhectic index [60]. Although large clinical studies are lacking, a variety of case reports have been reported [26, 35, 37] revealing a significantly increased propensity for cerebrospinal fluid dissemination [60], extra-CNS metastasis [63, 84, 89] and a possible benefit from platinum-based chemotherapy [57]. In addition, these tumours were reported to show an increased incidence of *TP53* alterations [92], *MYC/MYCN* amplification [60] and a peculiar profile of telomere maintenance mechanisms activation [34]. Recently two independent reports have shown that HGGs with a PNC component are particularly enriched by RB1 mutations [14, 74], suggesting that alterations in the RB1 pathway may represent a molecular hallmark for these entities. However, a clear hypothesis on the mechanisms responsible for this phenotypic skewing is still lacking. We hypothesised that HGGs with a PNC component may represent a unique model to investigate the relationships between genetic alterations, tumour biology and their phenotypic manifestations. Hereby, we extensively characterised a large cohort of HGGs with a PNC component by means of immunophenotypic and high-throughput molecular analyses. We demonstrate that both components display cell cycle deregulation and p53 pathway inactivation, but the PNC component displays further upregulation of transcriptional pathways associated with proliferative activity and increased tumour aggressiveness. Furthermore, we functionally characterised a gene product selectively expressed by the PNC component, Early B-cell Factor 3 (EBF3), which is directly controlled by MYC transcription factors in accessible chromatin sites and contribute to repress differentiation in a subset of glioma stem-like cell, thus promoting the development of the undifferentiated PNC phenotype.

Materials and methods

Sample collection

Newly diagnosed and pathologically confirmed HGGs with PNC component ($n=24$), medulloblastoma (MB; $n=15$), with either classical ($n=5$), desmoplastic/nodular ($n=5$) and large cell anaplastic ($n=5$) histology, and *IDH*-wildtype GBM ($n=15$), were retrieved from the Institutional database of the Pathology Service (Spedali Civili of Brescia). The cohort of "conventional" GBMs referred to as the reference cohort for the survival analysis has been previously reported in Orzan et al. [58]. Histological diagnosis was revised according to the WHO 2021 for CNS tumour classification criteria [3, 48] and formalin-fixed paraffin-embedded (FFPE) representative sections for each lesion were selected based on adequate tissue preservation, as assayed by Haematoxylin and Eosin (H&E) staining. For molecular analysis on the separated components, we selected cases displaying clearly distinguishable GBM and PNC areas and a sufficient amount of tissue. Using H&E-stained slides as a guide, GBM or PNC tumour cell-enriched areas were scraped from unstained 20-µm tissue sections and submitted to nucleic acid extraction (see further paragraphs). Information regarding clinical features, treatment and outcome were collected from the medical records. Genetic data concerning the general GBM population (TCGA GBM cohort) were

obtained from the public cBioPortal website (Glioblastoma Multiforme TCGA Firehose Legacy, https://www.cbioportal.org/) [11].

Immunohistochemistry

Briefly, 2-µm-thick FFPE tissue sections were de-waxed, rehydrated and endogenous peroxidase activity blocked with 0.3% H_2O_2 in methanol for 20 min. Heat antigen retrieval (when necessary) was performed using a microwave or a thermostatic bath in either 1.0 mM EDTA buffer (pH 8.0) or 1 mM Citrate buffer (pH 6.0). The sections were then washed in TBS (pH 7.4) and incubated for one hour or overnight in the specific primary antibody in TBS 1% bovine serum albumin (primary antibodies used are listed in Supplementary Table 1). The reaction was revealed by using Dako EnVision + Dual Link System Peroxidase (Dako Cytomation) followed by DAB and counterstained with Haematoxylin. For double and triple immunohistochemistry, after completing the first immune reaction, the second and third one were revealed by using MACH4 Universal AP Polymer kit (Biocare Medical) followed by Vector Blue kit (Vector) and StayRed kit (Abcam). Markers expression was semi-quantitatively scored on representative tumour regions based on both percentage [score ranges: 0 (0–5%), 1 (6–29%), 2 (30–69%), 3 (≥ 70%)] and intensity (score ranges: 0, no expression; 1, weak; 2, moderate; 3, high) of immunoreactive neoplastic cells with a combined cumulative score ranging from 0 to 6. The images were acquired with a Nikon DS-Ri2 camera (4908 × 3264 full-pixel) mounted on a Nikon Eclipse 50i microscope equipped with Nikon Plan lenses (× 10/0.25; × 20/0.40; × 40/0.65; × 100/1.25) using NIS-Elements 4.3 imaging software (Nikon Corporation).

IDH pyrosequencing assay and MGMT promoter methylation status

Genomic DNA was isolated from five 5-µm-thick FFPE tissue sections prior to assessment of adequacy of the sample and percentage of tumour cells. DNA extraction was performed by QIAamp DNA FFPE tissue (Qiagen) according to the manufacturer's protocol. The "IDH1/2 status" kit (Diatech) was used to identify the main variants in codon 132 of *IDH1* gene, exon 2 (R132H, R132L, R132C, R132G, R132S) and in codon 172 of *IDH2* gene, exon 4 (R172K). Pyrosequencing was carried out on a PyroMark system (Qiagen-Diatech) according to the manufacturer's protocol based on the "sequencing by synthesis" principle. Pyrograms outputs were analysed by the Pyromark ID 1.0 software (Biotage) using the Allele Quantification software to determine the percentage of mutant versus wildtype alleles according to percentage relative peak height. The evaluation of O6-methylguanine DNA methyltransferase (*MGMT*) promoter methylation status was performed by using "MGMT plus" kit (Diatech). DNA was subjected to polymerase chain reaction (PCR) amplification with a forward primer and a biotinylated reverse primer using the "MGMT PLUS" kit (Diatech Pharmacogenetics), according to manufacturer's instructions. Pyrosequencing methylation assay was performed in order to evaluate 10 CpG sites in the following regions: chr 10: 131,265,507–131,265,556 using sequencing primer of MGMT Kit (Diatech Pharmacogenetics). The data were analysed with the PyroMark CPG 1.0.11 (Qiagen) software.

Fluorescence and chromogenic in situ hybridization (FISH)

EGFR FISH was performed with the spectrum orange locus-specific identifier EGFR probe specific for the *EGFR* locus (7p12) and the DNA probe "Chromosome Enumeration probe" (CEP)7 specific for centromeric region of human chromosome 7 (7p11.1-q11.1, locusD7z1) labelled with fluorophore spectrum green (Abbott). *MYCN* FISH was performed with the ZytoLight SPEC MYCN/2q11 Dual Color Probe kit (ZytoVision). The ZyGreen SPEC MYCN probe is specific for the *MYCN* region of chromosome 2 (24p24.3) and the ZyOrange SPEC 2q11 probe is specific for the 2q.11.2 region of chromosome 2. Finally sections were counterstained with DAPI/Antifade Solution. All analyses were performed according to the corresponding manufacturer's protocols. Evaluation and scoring were determined according to criteria as previously described [15]. Images have been acquired by Nikon Eclipse 90i microscope using Genikon imaging software v 3.4.8. *EGFR* CISH was performed with the ZytoDot2C CEN EGFR/CEN7 Probe (ZytoVision) according to the manufacturer's protocol. The hybridization signal of digoxigenin-labelled polynucleotides appears as dark green coloured distinct dots (*EGFR* gene), and Dinitrophenyl-labelled polynucleotides appear as bright red coloured distinct dots (CEN7). Images were acquired by Aperio ScanScope® CS System for digital pathology (Leica Biosystems). Following CISH and image acquisition, immunostaining for GFAP was performed on the same slides and chromogen reaction was developed with Ferangi Blue Chromogen Kits (Biocare Medical). The images were then acquired again by Aperio ScanScope® CS System (Leica Biosystems).

Next generation sequencing

DNA from FFPE samples was obtained as previously described. BT483 DNA was extracted using the PureLink Genomic kit (Euroclone). DNA was fragmented using the M220 focused-ultrasonicator (Covaris®). The preparation of the NGS libraries started with End-Repair and A-Tailing

reactions, followed by adapter ligation (NXSEQ Amp-free Low DNA Library kit, Lucigen®; TruSeq™ DNA Single Indexes, Illumina). Then, the target of interest has been captured and enriched using the GBM-custom panel probes (xGen Predesigned Gene Capture Pools and xGen Hybridization and Wash kit, IDT®) following manufacturer's protocol. Final libraries were sequenced on MiSeq sequencer (Illumina®). We used a panel of genes designed to detect changes in 75 target genes whose alterations are known to be relevant for HGGs tumours (Supplementary Table 2). Custom-panel displays a genomic size as little as 196 Kbps. Genetic analysis was performed as reported in [18, 19, 91]. Briefly, sequences generated by Illumina MiSeq were pre-processed to remove all bases in the read with a Phred quality score less than 30. Reads were mapped to the human reference, assembly hg19, using BWA-mem algorithm. PCR duplicates were removed using the RMDUP command of SAMtools package. Custom pipeline for genetic analysis was used to call somatic variations when supported by at least 10% allelic frequency and 5% Fisher's Test significance level, according to previously published methods. Reads with more than three mismatches were filtered out. Insertions and deletions (indels) were identified using Pindel software and were annotated by custom scripts printing out gene information, number of normal and mutated reads, the allelic frequencies and the variation effect. Each of these entries was associated with the corresponding number of occurrences in the COSMIC database. Copy Number Variation (CNV) was obtained by calculating the ratio of median gene depth to the median depth of the whole exome. For each gene, copy number variation is reported as 2* tumour/normal CNV. The circular binary segmentation (CBS) algorithm, as implemented in the DNA copy R module, was used to cluster all the gene copy-number alterations. In the copy number analysis, a panel of 10 PBMCs was used as a normal reference.

RNA extraction and library preparation

RNA from FFPE samples was extracted using the Maxwell® RSC RNA FFPE Kit (Promega), according to the manufacturer's protocol. The RNA quality has been assessed using the RNA 6000 Nano kit (Agilent) on Bioanalyzer 2100 (Agilent) and quantified using the DNA HS Assay kit (LifeTechnologies) on Qubit (LifeTechnologies). Library preparation has been performed using TruSeq Stranded Total RNA Library Prep Gold (Illumina) which removes ribosomal RNA (rRNA) using biotinylated, target-specific oligos combined with Ribo-Zero rRNA removal beads. Following purification, the RNA was fragmented into small pieces using divalent cations under elevated temperature. The cleaved RNA fragments were copied into first strand cDNA using reverse transcriptase and random primers, followed by second strand cDNA synthesis using DNA polymerase I and RNase H. These cDNA fragments then have the addition of a single 'A' base and subsequent ligation of the adapter. The products were purified and enriched with PCR to create the final cDNA library. Libraries were quantified using Qubit (fluorometric assay) and quality evaluated using Agilent 2100 Bioanalyzer. Pooled libraries were sequenced on a NextSeq 500 system (Illumina) performing paired end sequencing 75 cycles run.

Gene expression quantification and data analysis

Each generated FASTQ file was aligned using STAR 2.5.1 [24] and mapped to the human GRCh38 genome reference. outFilterMultimapScoreRange was set to 3 to remove reads with ambiguous alignment GRCm38. The GENCODE release 27 was used as transcriptome reference annotation, and gene expression quantification was performed with featureCounts [44]. Functional characterization was performed by preranked GSEA [54, 78] exploring MsigDB signatures [45]. To perform Gliovis classification of RNAseq data from paraffin embedded samples we employed the single sample classifier from [58]. All the analyses were carried out on CPM data. Differential expression of TFs in the GBM vs PNC tumour components from patients was performed by filtering from the RNAseq raw counts the transcripts corresponding to human TFs, retrieved from https://humantfs.ccbr.utoronto.ca/cite.php [42], and by applying DESeq2 tool with LFC shrinkage [49]. TF transcripts with less than 10 counts were filtered out and significant differentially expressed TFs were selected based on p-adj > 0.1 e log2FC > = 0.5.

Methylation-based tumour classification and EBF3 promoter methylation analysis

FFPE tissue from the separated components of 4 GBM PNC tumours were collected into 1.5 ml and sent to Diagenode for DNA extraction and quality control. The Illumina Infinium Methylation EPIC array BeadChip (850 K) was carried out by the Epigenomic Services from Diagenode (Cat nr. G02090000). The output data (.idat files) were uploaded in the methylation-based classifier tool, version 12.8, available at https://www.molecularneuropathology.org/mnp/, as previously published [9]. Raw For EBF3 promoter methylation analysis, raw.idat files were analysed using the R package DMRcate [62]. Array type and probes annotation were performed, respectively, with Illumina Human Methylation EPIC manifest, Illumina Human Methylation EPICanno.ilm10b2.hg19 packages. Stratified quantile normalisation of data was performed to minimise unwanted variation was performed using minify package. Poor performing probes were filtered out based on: (i) p value greater than 0.05,

(ii) Sex associated chromosomes (Chr X and Chr Y), (iii) SNPs, (iv) Cross-reactive probes (list downloaded from https://genomebiology.biomedcentral.com/articles/https://doi.org/10.1186/s13059-016-1066-1). *M*-values were used to perform pairwise differential methylation analysis with False discovery rate lower than 5%.

Neurosphere culture and in vitro assays conditions

Neurospheres were previously obtained as described (L0512 [52]; BT483 [22]; GBM014 [21]). For their expansion, neurospheres were mechanically dissociated, counted with trypan blue to evaluate the number of live cells, and then re-plated as single cells at clonal density (1–10 cells/µl) in fresh medium. Neurospheres were kept in a medium containing DMEM/F-12 (Euroclone), 2 mM glutamine (Euroclone), penicillin–streptomycin (Euroclone), B-27 (Thermo Fisher Scientific). For L0512 and BT483 GSCs, human recombinant fibroblast growth factor 2 (bFGF, 20 ng/ml; Peprotech) and epidermal growth factor (EGF, 20 ng/ml; Peprotech) were added to the medium; GBM014, previously stabilised in the absence of growth factors [21], was maintained accordingly. The cells were incubated at 37 °C, 5% CO_2, H_2O saturated atmosphere. The cultures were checked monthly for mycoplasma infection using N-GARDE Mycoplasma PCR Reagent Set (Euroclone). Cell identity was periodically checked using PowerPlex® 16 HS System (Promega). For the invasion assay, 50,000 cells were plated in a round U-bottom 96 wells plate (Euroclone) and, the following day, cold, growth factors-deprived Cultrex® (R&D Systems) was added to the spheroids. Images were taken at T0 and at 24 h for L0512 and BT483 and 72 h for GBM014. The analysis was performed using ImageJ software, calculating the area and the perimeter of the spheroids at T0 and the total area of the spheroids at the selected time point (48 h). The area of the sprouts was calculated as the total area minus the spheroid area at T0. The relative sprouting area was derived as the ratio: sprouts area/spheroid perimeter.

Organoids culture

The method for establishing organoids was based on the protocol as reported in Hubert et al. [33]. Briefly, 100.000 GSCs were resuspended in 10 µl of Corning Matrigel Matrix for Organoids Culture (Merck) and seeded in a dimple made in a piece of sterile parafilm. Once polymerized, the drops were transferred in a Petri well in standard growth medium for 2 weeks. Organoids were manually detached from the bottom of the dish daily and fresh medium was added twice a week. After 2 weeks, organoids were formalin fixed and paraffin embedded for histological analysis as previously described.

Cell blocks preparation

2 million cells were resuspended in physiological solution (NaCl 0.9%); plasma and thromboplastin were added dropwise until the formation of a clotted sphere. The sphere was immediately formalin fixed and paraffin embedded. Cell blocks were cut into 2 µm sections and processed for IHC as previously described.

Sanger sequencing for *TP53* alterations

In L0512 *TP53* (full coding sequence) from genomic DNA, extracted with the PureLink Genomic kit (Euroclone), was amplified using Platinum® Taq DNA Polymerase (Thermo Fisher Scientific) and specific primer pairs (Supplementary Table 3). PCR conditions were as follows: 95 °C for 3′; 3×[95 °C for 15″, 64 °C for 30″, and 70 °C for 1′]; 3×[95 °C for 15″, 61 °C for 30″, and 70 °C for 1′]; 3×[95 °C for 15″, 58 °C for 30″, and 70 °C for 1′]; 37×[95 °C for 15″, 57 °C for 30″, and 70 °C for 1′]; and 70 °C for 5′. PCR products were purified using Illustra™ ExoProStar 1-Step (Merck) according to manufacturer's instructions. Sequencing was performed using BigDye Terminator v3.1 Cycle Sequencing kit (Thermo Fisher Scientific); sequencing products were purified using CleanSEQ Dye-Terminator Removal Kit (Beckman Coulter) and analyzed with a 3730 DNA Analyzer ABI capillary electrophoresis system (Thermo Fisher Scientific). Data were visualized by Chromas Lite 2.66 software (http://www.technelysium.com.au/chromas_lite.html) and compared with reference sequences from the Homo sapiens assembly GRCh37. All identified variants were analysed for possible pathogenicity using MutationTaster2021 [75] and compared with those in the Catalogue Of Somatic Mutations In Cancer (COSMIC, https://cancer.sanger.ac.uk/cosmic) and in The TP53 Database (https://tp53.isb-cgc.org/).

Gene copy number evaluation

Gene copy number analysis of L0512 DNA, extracted using the PureLink Genomic kit (Euroclone), was assessed by real-time PCR, using TaqMan Universal PCR Master MIX and the ABI PRISM 7900HT sequence detection system (Thermo Fisher Scientific). Primers/probes for TaqMan copy number assays are reported in the Supplementary Table 3). Relative gene copy number data were calculated by normalising against endogenous control (RNaseP). Normal diploid human gDNA (PBMCs) was used as a calibrator to obtain the ΔΔCt. The copy number of each gene was calculated with the formula $2\times2^{-\Delta\Delta Ct}$. Gene amplification is defined when copy number is > 5; heterozygous deletion is defined when copy number is < 1.5; copy number gain is defined when copy number is 3 < CN < 5. *CDKN2A* homozygous

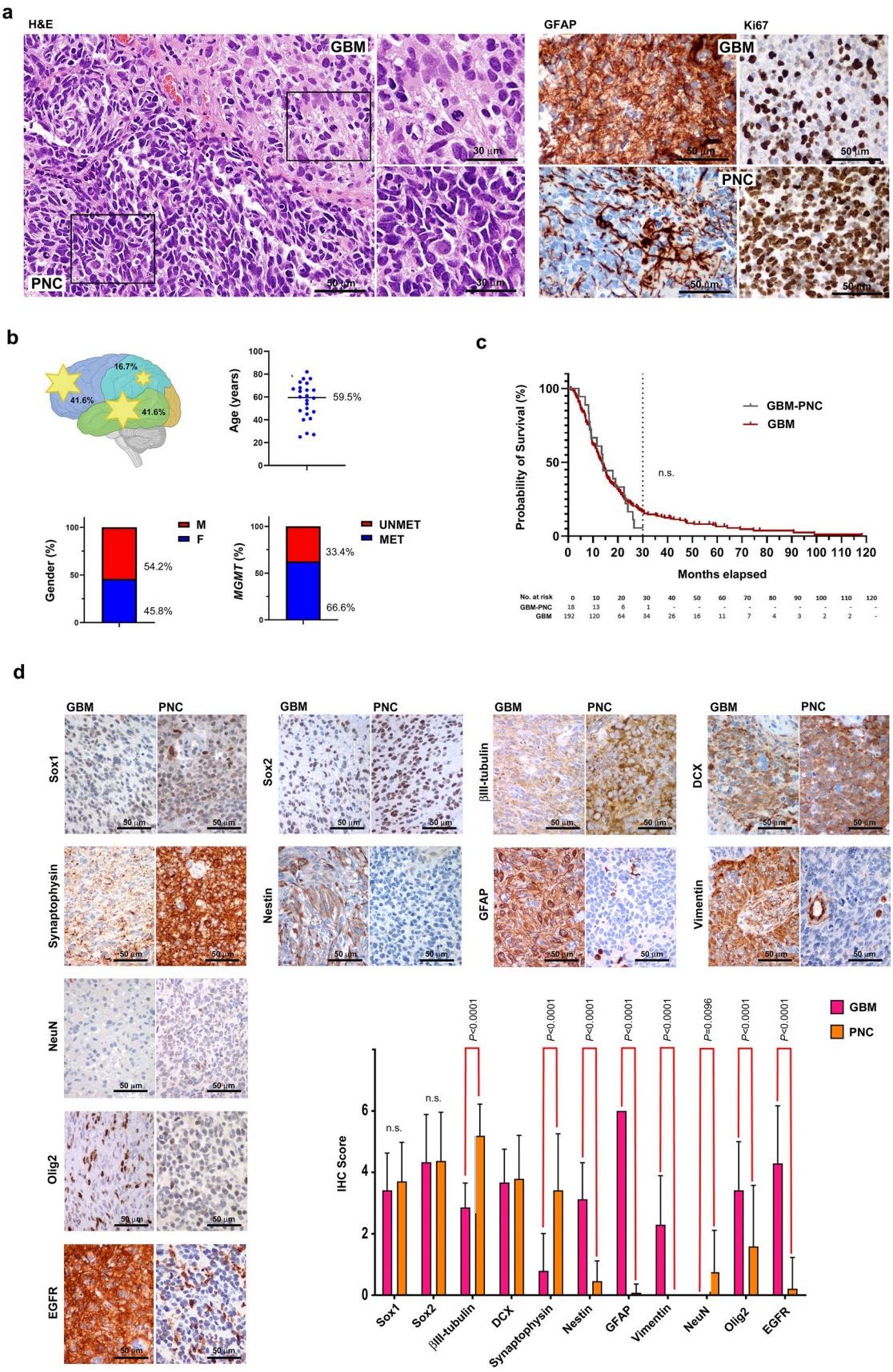
a
H&E
GBM
PNC
GFAP
Ki67
b
16.7%
41.6%
41.6%
Age (years)
59.5%
Gender (%)
M
F
54.2%
45.8%
MGMT (%)
UNMET
MET
33.4%
66.6%
c
Probability of Survival (%)
GBM-PNC
GBM
n.s.
Months elapsed
No. at risk
GBM-PNC
GBM
d
Sox1
Sox2
βIII-tubulin
DCX
Synaptophysin
Nestin
GFAP
Vimentin
NeuN
Olig2
EGFR
IHC Score
P<0.0001
P=0.0096
n.s.

◂**Fig. 1** GBM-PNC clinical features and immunophenotypical characterization. **A** Representative H&E image of the bi-phasic histology of a GBM-PNC (left panels). Insets show details of the GBM (upper) and the PNC (lower) components. Immunohistochemistry for GFAP and Ki-67 of representative GBM and PNC components, respectively, of a GBM-PNC tumour are shown (right panels). **B** Clinical features of the patient cohort showing the preferential sites of involvement (upper left), median age at diagnosis (upper right), gender (lower left) and MGMT methylation status (lower right). **C** Kaplan–Meier overall survival curves of patients with GBM-PNC ($n=18$) as compared to a conventional GBM cohort ($n=192$). Log-rank test was performed. **D** Representative immunohistochemical stainings showing the phenotypical profile of GBM-PNC of the study cohort with a panel of neurogenesis-related markers. The plot displays the evaluation and scoring determined according to criteria stated in the Material and Methods section. Error bar represents mean ± s.d., two-tailed, unpaired Student's *t*-test

deletion in L0512 corresponds to the absence of CDKN2A signal in the presence RNaseP signal.

CRISPR-mediated genome editing

CRISPR/Cas9-mediated genome editing was used to generate clonal EBF3 knockout GSCs. The gRNA chosen sequence was designed using the online resource: https://chopchop.cbu.uib.no/. The gRNA sequence was cloned into LentiCRISPRv2GFP (gift from David Feldser, Addgene plasmid #82,416; http://n2t.net/addgene:82416; RRID:Addgene_82416) following the protocol provided by the Zhang's laboratory, available on https://www.addgene.org/crispr/reference/#protocols [71]. Lentiviral production was performed as previously reported [87]. Clonal BT483 and GBM014 colonies were screened for GFP expression and for EBF3 expression by western blot. Genomic DNA was extracted from the clones using the PureLink Genomic kit (Euroclone) following manufacturer's instructions and genomic alterations were confirmed by Sanger DNA sequencing. PCR products were purified using EuroSAP PCR Enzymatic Clean-up kit (Euroclone). Cycle sequencing was carried out using BigDye Terminator v3.1 Cycle Sequencing kit (Applied Biosystems). Sequencing products were purified using Performa® Spin Columns (Edge BioSystems) and analysed on a 3130 DNA Analyzer ABI capillary electrophoresis system (Applied Biosystems). Sequences were then analysed using Chromas Lite 2.66 software (http://www.technelysium.com.au/chromas_lite.html).

Stable cell transfection with EBF3

GBM CSCs (L0512) were transduced with a lentiviral vector coding for EBF3, as previously described [17]. Sister cultures were infected with pCCL.sin.cPPT.PGK.GFP.WPRE11, as a mock condition. Clones were screened by RT-qPCR and western blot for EBF3 expression. Total RNA was extracted by the Trizol method (Ambion, Thermo Fisher Scientific) following manufacturer's instructions. Purified nucleic acids were quantified with Nanodrop mySPEC (VWR) and used for downstream applications. 1 µg of total RNA was submitted to a reverse-transcription reaction using iSCRIPT cDNA synthesis kit (Bio-Rad). RT-qPCR was performed on a ViiA7 Thermal cycler using Gene Expression Taqman® with the Fast Advanced Master Mix (Thermo Fisher Scientific) system. Glyceraldehyde-3-phosphate dehydrogenase (GAPDH) mRNA was used as an endogenous reference for the relative quantification.

Western blot

Cells were scraped from dishes in ice-cold lysis buffer containing phosphatase and protease inhibitor cocktail (Thermo Fisher Scientific). Proteins were quantified using the Bradford protein assay (Euroclone). 40 µg of proteins were resolved by SDS-PAGE using Bolt™ 8%-10% Bis–Tris Plus pre-cast gels, then transferred to PVDF Transfer Membrane (Thermo Fisher Scientific). The primary antibodies used for immunoblotting assay are listed in Supplementary Table 1. After incubation with horseradish peroxidase-conjugated secondary antibodies (Euroclone), membranes were developed with ECL Star Enhanced Chemiluminescent Substrate (Euroclone) and visualised with LI-COR Imaging System (Odyssey). Band intensity was quantified by densitometric analysis using ImageJ software.

Selection of putative MYC binding sites on EBF3 locus

Primers for target regions of EBF3 gene were designed based on the integration of: (i) ENCODE Transcription Factor ChIP-seq Clusters, available from UCSC Genome browser (Human Grch37); (ii) Previously published ATAC-seq and H3K27ac ChIP-seq data for LUHMES cells (high EBF3 expression) that were available on GEO (accession nr. GSE109706 and GSE125658); and (iii) best matching Transcription factor motifs (p-value $< 3 \times 10^{-5}$), calculated using FIMO tool on HOCOMOCO v11 database (Grch37) of transcription factor motifs available from MEME database (https://meme-suite.org/meme/doc/download.html), filtered by the list of the top 150 PNC upregulated transcription factors. Six putative MYC binding sites were selected according to the above parameters, of which three are in the gene body (here named BS2 n1, BS2 n2, BS1), one is within the promoter region (named Promoter), and two are upstream of the gene in putative enhancer regions (named Enh n1 and Enh n2). The corresponding primer sequences are listed in the Supplementary Table 3.

Table 1 Clinical features of the study cohort

Characteristic	(No. 24) No. (%)
Gender	
Female	11 (45.8)
Male	13 (54.2)
Age, years (median 59.5 years)	
< 65	14 (58.3)
≥ 65	10 (41.7)
Site	
Frontal	10 (41.6)
Parietal	4 (16.7)
Temporal	10 (41.6)
Follow-up	
Short-term recurrences	6
Cranio-spinal diffusion	4
Extra-CNS metastasis	1

Chromatin immunoprecipitation and qPCR

ChIP experiments were performed on L0512, GBM014 and BT483 wildtype GSCs. For each sample 1×10^6 cells were cross-linked with 1% formaldehyde for 10 min at RT. The reaction was quenched by addition of glycine at a final concentration of 0.125 M. Cells were lysed in lysis buffer upon incubation for 5 min on ice and then chromatin was sonicated using a Covaris M220 with the following settings: peak power 75 W, duty factor 10, cycles burst 250, time 1020 s. The samples were centrifuged for 10 min at 10′000xg to remove cellular debris. The sonicated chromatin was precleared with protein G coated magnetic beads (Invitrogen) and 5% of the material was saved as input DNA. The remaining material was incubated for 4 h at 4 °C with protein G coated magnetic beads, previously functionalized with the antibodies listed in Supplementary Table 1. After washing of the non-specific binding to the beads, the immunoprecipitated DNA was purified using AMPure XP beads (Backman coulter) and analysed by qPCR by using SYBR GreenSensiFAST SYBR kit (Bioline) and primers amplifying six putative MYC binding sites. The selected region qPCR values were represented as percentage of Input after correction for the dilution factor.

EBF3 promoter methylation-specific PCR

Genomic DNA was extracted from L0512, BT483 and GBM014 cell lines with standard salt-extraction and precipitation. Bisulfite modification was performed using 200 ng of DNA with the EZ DNA methylation kit (Zymo Research #D5001) in order to convert unmethylated cytosines to uracils. The modified DNA was then purified using the Wizard DNA Clean Up System (Promega, Madison, WI, #A9281). An equal amount of purified DNA for each sample was subjected to 40 cycles PCR using specific primer sets that discriminate between unmethylated and methylated promoter regions of EBF3 (Supplementary Table 3) [39]. PCR products were run on a 1.5% agarose gel and visualised at a ChemiDoc Imager (BioRad). Quantification of PCR bands was performed using ImageJ software. The experiment was performed in four biological replicates.

Statistics and reproducibility

Statistical comparisons were performed using the unpaired two-sided Student's *t*–test, one-way or two-way Analysis of Variance (ANOVA) and Fisher's exact test. Survival curves were analysed using the Kaplan–Meier method and the non-parametric log-rank (Mantel–Cox) test. Data were presented as the mean ± standard deviation of at least three independent experiments, unless otherwise stated in the figure legend. Statistical analyses were performed using GraphPad Prism Software 8.4.3 (GraphPad Software Inc.) and p-value < 0.05 was considered as statistically significant. $^*p < 0.05$; $^{**}p < 0.01$; $^{***}p < 0.001$; $^{****}p < 0.0001$.

Results

Patient cohort and clinical features

This study was conducted on 24 newly diagnosed HGGs with a PNC component upon revision of histological diagnosis, hereby referred to as GBM-PNC since the large majority of cases were *IDH*-wildtype (20 out of 24). The study cohort was selected based on rigorous histological criteria including: (i) presence of a malignant glial component with histological features of "conventional" GBM; (ii) well recognizable nodules reminiscent of a primitive neuroectodermal tumour (PNET) with loss of GFAP expression and composed of poorly differentiated cells with hyperchromatic nuclei, high N/C ratio, severe anaplasia and abundant mitotic figures, corresponding to an extremely high Ki-67 proliferation index (Fig. 1A). We did not consider cases with undifferentiated GFAP-negative components without clear PNET-like features. Clinical features of the patients are reported in Table 1, Supplementary Table 4 and Fig. 1B. The median Overall Survival (OS) for the whole study cohort (available for 18 cases out of 24) was 13.9 months, in line with the OS of conventional GBMs (13.6) as reported by our previously published cohort of patient ($n = 192$), hereby considered as reference cohort[58]. However, the survival rate at 30 months post-diagnosis for GBM-PNC was only 5.5% (1/18) as compared to conventional GBMs (17.7%; 34/192) (Fig. 1C). Of note, according to the high aggressive

behaviour of GBM-PNC, 25% of patients (6/24) developed short-term recurrences, four patients showed cranio-spinal dissemination and 1 patient developed additional extra-CNS multiple metastasis to liver and bones.

GBM-PNCs show either common or mutually exclusive biomarker expression within the two components

As described above, GBM-PNCs are characterised by a mixed phenotype composed of a glial component (GBM) associated with nodules of immature cells that display an early neuronal differentiation (PNC). During embryonic development, neurogenesis regulates differentiation of glial and neuronal cells from a common stem progenitor cell. To highlight common or distinctive features for each of the two components we investigated a large panel of markers expressed by differentiating progenitors during neurogenesis at different maturation stages (Supplementary Fig. 1a and Supplementary Table 4). As illustrated in Fig. 1D, both components display an immature profile, as shown by the comparable expression levels of Sox1 and Sox2, considered early markers of differentiation commonly expressed by stem and early progenitor cells. Interestingly, the early neural differentiation-related gene Doublecortin (DCX) [2, 94] was also found to be expressed in both components, albeit with slightly higher intensity in the PNC component. We then evaluated the expression of markers associated with either glial or neuronal differentiation. As expected, Synaptophysin, an integral membrane glycoprotein expressed in the presynaptic vesicles in neurons and widely recognized as a sensitive marker of neuronal or neuroendocrine differentiation in various tumours [27], was mainly expressed in the PNC component, according to the evidence that Synaptophysin expression occurs early in neurogenesis and is associated with an early step of neuronal differentiation [90]. Of note, βIII-tubulin was found to be expressed at a significantly higher level in the PNC component, according to its key role in promoting neuronal differentiation, while the neuronal marker NeuN, associated with a mature neuronal phenotype, was substantially negative or detected at very low levels only within the PNC component. In addition, the tumours frequently showed a diffuse and strong nuclear immunoreactivity for the transcription factor TTF1 (clone SPT24; 10 out of 16 cases; 62.5%) that was selectively expressed in the PNC component, as previously reported [80] (data not shown). Conversely, well known biomarkers associated with the glial phenotype and usually expressed in GBMs, such as GFAP and Vimentin, were exclusively expressed in the glial component, even at variable levels. Interestingly, Nestin, a recognized marker of Neural Stem Cells (NSC) [4, 94], was also significantly expressed in the GBM component, while barely detected within the PNC portion of the tumour (Fig. 1D), in line with the observation that a subset of radial glial precursor cells in the developing human brain co-express both Nestin and GFAP [4, 38, 41, 70] and fortify the concept that the GBM component retains an immature phenotype. In addition, Olig2, a transcription factor previously linked to the oligodendroglial lineage but widely considered a proneural glioma-associated marker [81], was highly expressed in the GBM component, but barely detected in the PNC component (Fig. 1D). Of note, expression of EGFR was mostly confined to the GBM component, while extremely low and hardly detected in the PNC component (Fig. 1D). As previously reported, EGFR overexpression in GBM strictly correlates with gene amplification/polysomy while cases with low or negative EGFR expression are mostly considered not amplified [15]. We thus performed FISH analysis in the EGFR overexpressing samples (14/24 samples; IHC score 5 or 6). As expected, in the GBM component *EGFR* was amplified/polysomic in all of the cases with IHC score 6 ($n=10$) and in 2 cases with IHC score 5 ($n=4$) (Supplementary Fig. 1b). Unexpectedly, in eight cases *EGFR* appeared to be amplified/polysomic also in the PNC component, regardless of weak or negative EGFR expression. Since FISH analysis does not allow to clearly discriminate the morphology of the two components, frequently intermixed, we performed CISH analysis combined with IHC for GFAP in four representative samples out of 14 (3 amplified and 1 non amplified). In the three amplified samples, we confirmed chromosome 7 amplification in both components (Supplementary Fig. 1c and Supplementary Table 4). Interestingly, EGFR transcript, as assayed by RNA sequencing in 8 samples out of 14, was retained in both components regardless of the EGFR protein expression and/or amplification/polysomy, suggesting that, although EGFR amplification and mRNA expression are shared by both components, EGFR protein expression in the PNC component is inhibited by post-transcriptional mechanisms (Supplementary Fig. 1d and Supplementary Table 4). Since EGFR is a key molecule driving gliomagenesis [51, 52], suppression of EGFR expression in the PNC component is in keeping with the PNC phenotype determination.

Transcriptional profile reveals that PNC component has a remarkable enrichment in the neural progenitor cell phenotype, MYC targets and RB1 pathway downregulated genes

To systematically explore the gene transcriptional profile of both GBM and PNC components, we performed RNAseq profiling of the separated components from 10 patients of our cohort, together with 14 GBMs with known transcriptional subtype, used as a reference cohort [15]. Transcriptional subtyping based on the canonical proneural-classical-mesenchymal signature [58, 88] showed that, in 3/10 GBM-PNC tumours, both components displayed a proneural

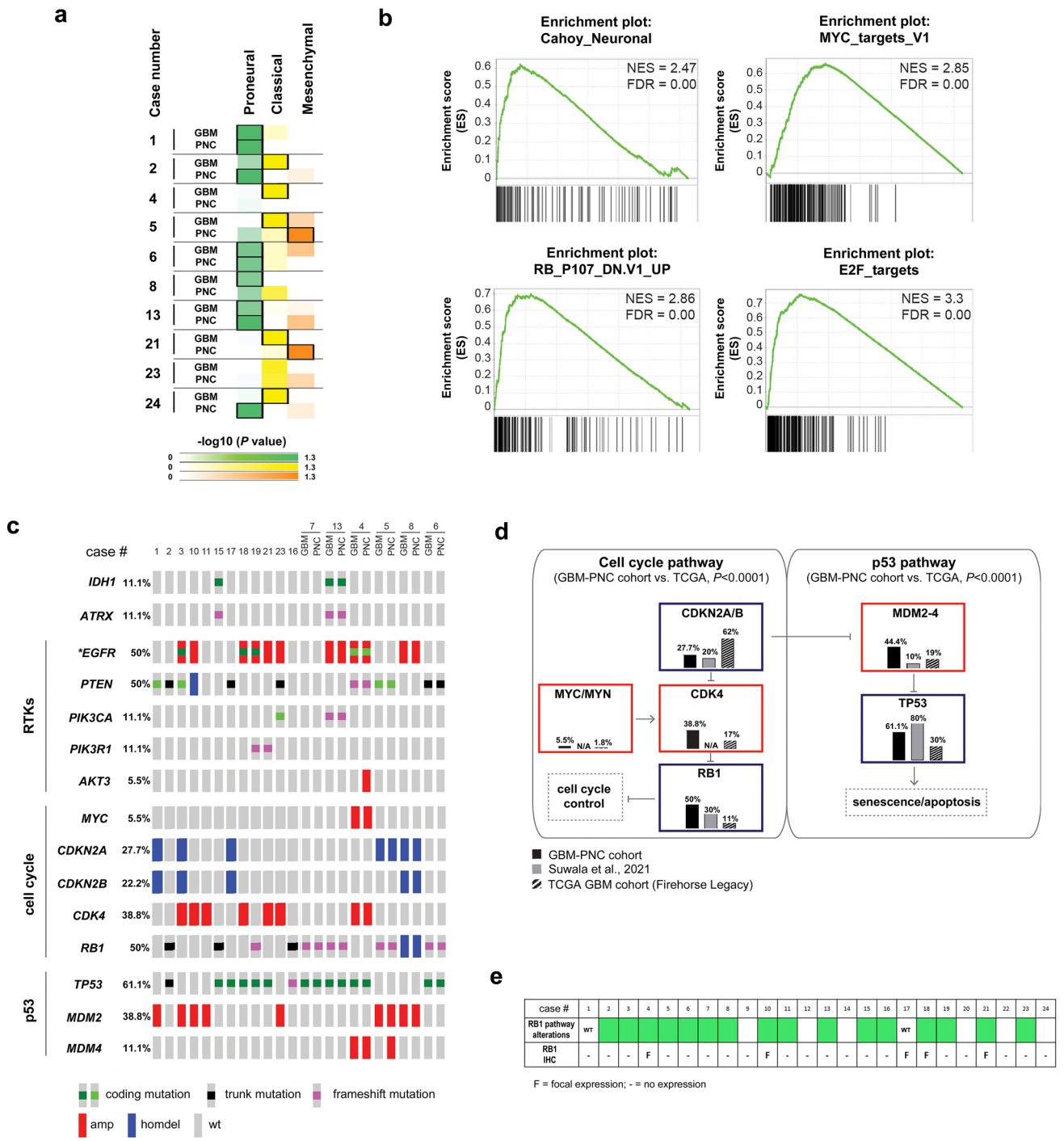

profile. In the remaining 7/10 tumours, the GBM component was either classical ($n = 5/7$) or not assigned ($n = 2/7$), while the PNC component was either proneural ($n = 2/7$), or mesenchymal ($n = 2/7$), or classical ($n = 1/7$), or not assigned ($n = 2/7$) (Fig. 2A, Supplementary Fig. 2a and Supplementary Table 5). Although this sample panel is too small to draw statistically significant conclusions, we can observe that PNC components preferentially display a proneural phenotype ($n = 5/10$), while the classical profile, whose frequency is prominent in the GBM component as well as in the general GBM population [88], is underrepresented ($n = 0/10$). Gene Set Enrichment Analysis (GSEA) based on MSigDB collections, including C6 (oncogenic gene sets), H (hallmarks gene sets) and TFT (all transcription factor targets) revealed a striking enrichment of some gene sets in the PNC vs. GBM components, in particular the Cahoy neuronal signature [8], MYC targets, genes upregulated by RB1 loss, and E2F targets (Fig. 2B and Supplementary Table 6).

◂**Fig. 2** Transcriptional and molecular characterization of the tumour cohort. **A** Heatmap showing the classification of GBM and PNC components of each of the indicated tumours (10 out of 24) into proneural, classical or mesenchymal subtype. Colour intensity is proportional to probability of subtype assignment. Outlined squares indicate significant subtype assignment ($P < 0.05$). Colour legends for −log10 (P values) are shown. **B** Gene set enrichment analyses of Cahoy neuronal signature [8], MYC targets, RB1 downregulated genes and E2F targets in the PNC vs. the GBM component of tumours as in **A** *NES* normalised enrichment score; *FDR* false discovery rate. **C** Oncoprint showing genetic alterations in the main GBM oncogenic pathways in 18 out of 24 cases of our GBM-PNC cohort, analysed by NGS. In 6 out 18 samples the two GBM and PNC components were analysed separately. Overall frequency and type of each alteration is indicated. *EGFR amplification frequency results from a combination of NGS and FISH data (see also Supplementary Fig. 2). **D** Comparison between the frequency of each genetic alteration found in 18 out of 24 cases of our GBM-PNC cohort, the GBM-PNC cohort reported by Suwala ($n = 20$)[80] and the TCGA-GBM cohort ($n = 273$). Enrichments in cell cycle and p53 pathway mutations in our GBM-PNC cohort vs. the TCGA GBM cohort are statistically significant (Fisher's exact test, $P < 0.0001$). **E** Table showing the comparison between the presence of molecular alterations in RB1 or CDK4 and IHC staining for RB1 in the 24 GBM-PNC tumours of the study cohort

Enrichment in the Cahoy neuronal signature is consistent with the neural progenitor cell phenotype indicated by IHC profiling. Enrichments in MYC targets, genes upregulated by RB1 loss, and E2F targets are coherent with the increased proliferative index observed in the PNC component by Ki67 IHC staining (Fig. 1A), as previously reported [60].

GBM-PNC components are both highly enriched in RB1 and p53 pathway genetic alterations

We analysed the genetic alterations of 18/24 GBM-PNC cases in our cohort, using a custom NGS panel designed to explore 75 genes related to GBM (Supplementary Table 2). To investigate a possible genetic basis for intratumoral phenotypic heterogeneity, NGS was performed on the separated GBM and PNC components of only 6 cases, due to the difficulty to sharply dissect the two different components, frequently intermixed (Fig. 2C). No significant genetic differences were reported between the GBM and the PNC component. However, NGS revealed that the GBM-PNC genetic landscape is significantly different from that of the conventional GBM population (TCGA GBM cohort) (Fig. 2C and D and Supplementary Table 7). In GBM-PNCs we observed reduced frequency of *CDKN2A/B* deletion (5/18 cases, i.e. 27.7% vs. 62% in the TCGA GBM cohort), and strikingly increased frequencies in alterations of the cell cycle control and p53 pathways (Fig. 2C and D and Supplementary Table 7). All cases presented at least one alteration of a cell cycle control gene, in particular *RB1* trunk or missense mutation or deep deletion (9/18, i.e. 50% vs. 11% in the TCGA GBM cohort), or *CDK4* amplification (7/18, corresponding to 38.8% vs. 17% in the TCGA GBM cohort). Concerning the *TP53* pathway, all cases displayed either a *TP53* mutation (11/18, i.e. 61.1% vs. 30% in the TGA GBM cohort) or *MDM2-4* amplification (8/18, i.e. 44.4% vs. 19% in TCGA cohort) (Fig. 2C and D). The frequencies of such genetic alterations in our cohort were similar to those reported in GBM-PNC by Suwala et al. (Fig. 2D) [80]. Immunohistochemical analysis complemented by pyrosequencing confirmed the presence of *IDH1* R132H mutation in 2/18 cases analysed by NGS, and detected the alteration in 2 additional samples in our cohort (Supplementary Table 4), indicating that the PNC phenotype may associate with both an *IDH*-wildtype and an *IDH*-mutated background (Supplementary Fig. 3a and b). IHC also confirmed the presence of overexpressed p53 in *TP53* mutated samples, as described [82] (Supplementary Fig. 3a and c). Interestingly, IHC showed that *RB1* mutated (9/18), *CDK4* amplified (7/18) and additional cases not analysed by NGS were negative for RB1 expression, or displayed only a focal expression (Fig. 2E and Supplementary Fig. 3d). These data indicate that the highly frequent *RB1* or *CDK4* alterations were associated with loss of RB1 expression (complete in the case of *RB1* mutation), likely resulting in the loss of restrictions on cell cycle progression. Interestingly, methylation profiling, performed on the separated components in 4 representative samples (including 3 *IDH*-wildtype HGGs and 1 *IDH* mutant HGGs with a PNC component) using the latest (v12.8) version of the brain tumour classifier, assigned the same methylation class to both GBM and PNC components. Two of the *IDH*-wildtype HGGs were classified to the methylation class of Glioblastoma with PNC component and the *IDH*-mutant HGG was identified as astrocytoma *IDH*-mutant, high grade. The remaining *IDH*-wildtype HGG did not show any matches due to a low calibrated score (Supplementary Fig. 3e). Of note, the copy number profile obtained from the algorithm for all the four samples analysed revealed relevant chromosomal aberrations particularly related to the TP53 and RB1 pathways, such as gain of MDM2-4 and CDK4 and loss of RB1 (Supplementary Fig. 3f). Taken together, these data confirm a strong involvement of the RB1 pathway in PNC phenotype determination. However, since the NGS analysis of separated GBM and PNC fractions displays a high degree of concordance, and a strong enrichment in *RB1* mutation Variant Allele Frequency (VAF) or *CDK4* amplification levels in the PNC component compared to the respective GBM component was observed only in two cases, the RB1 pathway alterations should be considered only as a predisposing factor for GBM-PNC onset rather than a determinant of the PNC component.

EBF3 is selectively expressed in the PNC component and is associated to an early neuronal, rather than a glial phenotype

Since transcriptional data showed an enrichment in the Cahoy neuronal signature in the PNC component, we

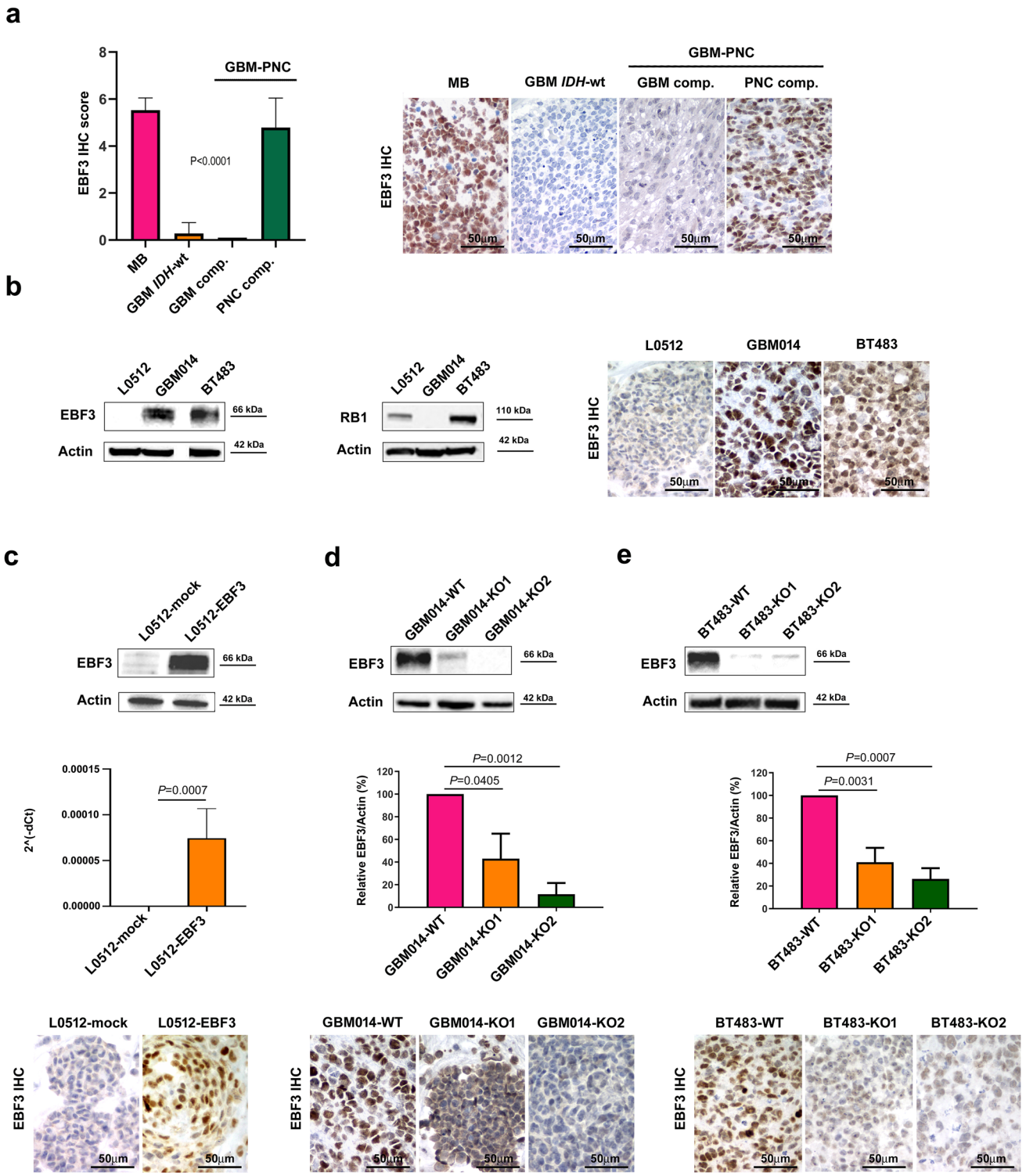

searched for a neuronal development-related gene that could be accountable for the PNC phenotype. Among the likely candidate genes we chose *EBF3*, a transcription factor expressed during mouse embryogenesis in early post-mitotic neurons with a regulatory function in neuronal differentiation and maturation [72], that analysis of the differentially expressed genes between GBM and PNC components highlighted as significantly upregulated in the PNC component. Indeed, we have previously reported that EBF3 is expressed in human medulloblastoma, a malignant cerebellar embryonal tumour with early neuronal differentiation, while being consistently negative in GBMs [17]. Of note, sustained

◂**Fig. 3** EBF3 expression in CNS tumours and creation of an in vitro model for the study of its function. **a** Left: EBF3 IHC expression score in a cohort of medulloblastoma (MB) ($n=15$), GBM *IDH*-wiltdtype ($n=15$) and in the GBM and the PNC distinct components of the tumour study cohort ($n=24$). Evaluation and scoring were determined according to criteria stated in the Material and Methods section. Right: representative images of EBF3 IHC in, from left to right, a MB, a GBM *IDH*-wildtype, the GBM and the PNC components of a GBM-PNC (case #15). Statistical significance was determined by one-way ANOVA test. **b** Selection and characterization of 3 GSCs based on EBF3 and RB1 expression as assessed in Western Blot (left) and IHC on cell blocks (right). **c** Upper: Western Blot for EBF3 in control and transduced L0512 GSCs. Central: RTqPCR for EBF3 in control and overexpressing L0512 clones. The levels of mRNA are expressed as 2^(−dCt) related to GAPDH. Lower: representative EBF3 IHC on cell blocks of control and overexpressing L0512 clones. **d** Upper: Western Blot for EBF3 in control and knockout GBM014 clones. Central: quantification of EBF3 expression in control and knockout GBM014 clones. Lower: representative EBF3 IHC on cell blocks of control and knockout GBM014 clones. **e** Upper: Western Blot for EBF3 in control and knockout BT483 clones. Central: quantification of EBF3 expression in control and knockout BT483 clones. Lower: representative EBF3 IHC on cell blocks of control and knockout BT483 clones. Error bar represents mean ± s.d. of $n=3$ independent experiments, two-tailed, unpaired Student's *t*-test

EBF3 expression correlates with an immature phenotype and promotes neoplastic progression. Since accessibility to embryonic and foetal tissue is limited and mouse models lack human-specific features critical for human neurogenesis, we investigated the time course of EBF3 expression during neurogenesis in immature human teratoma samples, a recognized model of human neurogenesis in vivo [61]. Actually, the neural elements of surgically resected teratomas faithfully recapitulate the early stages of human CNS development by forming embryoid bodies and neuroectodermal structures [50, 83]. We found that EBF3 is specifically expressed in the βIII-tubulin + transitional areas between immature and mature neuroblasts within the external layer of the primitive neuroectodermal tubules, while it is not expressed within the primitive tubules of the immature Sox2 + neuroectodermal component or in the mature NeuN + neurons and in the committed GFAP + glial components (Supplementary Fig. 4). We then investigated EBF3 expression in our cohort of GBM-PNC along with medulloblastomas ($n=15$), as positive controls, and conventional GBM IDH-wildtype ($n=15$), as negative controls. Data showed that EBF3 is highly expressed in the PNC component of GBM-PNC, while consistently negative in the GBM component (Fig. 3a), designating EBF3 as a valuable marker associated with an early neuronal rather than glial phenotype.

EBF3 expression hampers GSCs glial differentiation favouring a cell fate toward an early neuronal specification and onset of a biphasic phenotype with increased invasive capacity

To investigate the putative role of EBF3 in GBM-PNC and the molecular mechanism underlying its exclusive upregulation in the PNC component, we identified three glioma stem cell (GSC) cultures (neurospheres) from a set available in our laboratory, based on EBF3 and RB1 expression (Fig. 3b). As representative of conventional GBM, we identified L0512 GSCs, previously described in Mazzoleni et al. [52], which were negative for EBF3, retained RB1 expression and did not display any copy number alteration in *RB1*, *MYC*, *MYCN* and *CDK4* genes, while harbouring *CDKN2A* homozygous deletion and *TP53* p.R273L mutation (Supplementary Fig. 5a). As representative of GBM-PNC, we identified two GSCs that expressed EBF3 while exhibiting lack of RB1 expression and TP53 mutation. GBM014 GSCs, derived from a previously diagnosed GBM-PNC primary tumour, harboured a hemizygous trunk mutation of the *RB1* gene together with *CDKN2A* and *MYC/MYCN* wild-type genes (Supplementary Fig. 5a) [21]. BT483 GSCs, chosen within a panel of previously characterised 98 neurospheres, displayed *RB1* wild-type genes but harboured a *MYCN* amplification, likely leading to RB1 functional down-regulation, along with CDKN2A wild-type gene (Supplementary Fig. 5a) [21, 22]. We then engineered GBM GSCs L0512 to stably overexpress EBF3, obtaining L0512-EBF3 and the corresponding EBF3-negative control GSCs (L0512-mock), in which the expression levels of EBF3 were assessed both at transcriptional and protein level (Fig. 3c). We also engineered GBM-PNC GSCs GBM014 and BT483 to knock-out EBF3 gene using the lentiviral CRISPR/Cas9 technology with a sgRNA targeting the exon 8 of *EBF3* gene (Supplementary Fig. 5b). For each GSC culture, 1 wildtype pool (GBM014-WT and BT483-WT) and 2 knockout clones (heterozygous GBM014-KO1 and homozygous GBM014-KO2, BT483-KO1 and BT483-KO2) were selected and screened by Sanger sequencing (Supplementary Fig. 5c). Expression of EBF3 was assayed at protein level (Fig. 3d and e). We then investigated how the gain or loss of EBF3 expression impacts on the phenotype of the transduced GSCs in proliferative conditions. Since GBM-PNC tumours have a dual glial and primitive neuronal phenotype, we assessed the expression of GFAP as a glial marker and βIII-tubulin as an early neuronal marker. The EBF3-transduced GSCs (L0512-EBF3) expressed lower levels of GFAP as compared to their parental counterpart (L0512-mock) (Fig. 4a). Accordingly, the EBF3-knockout clones GBM014-KO2, BT483-KO1 and BT483-KO2 exhibited higher GFAP expression levels as compared to the respective parental controls (GBM014-WT, BT483-WT), as assayed by both WB and IHC on cell

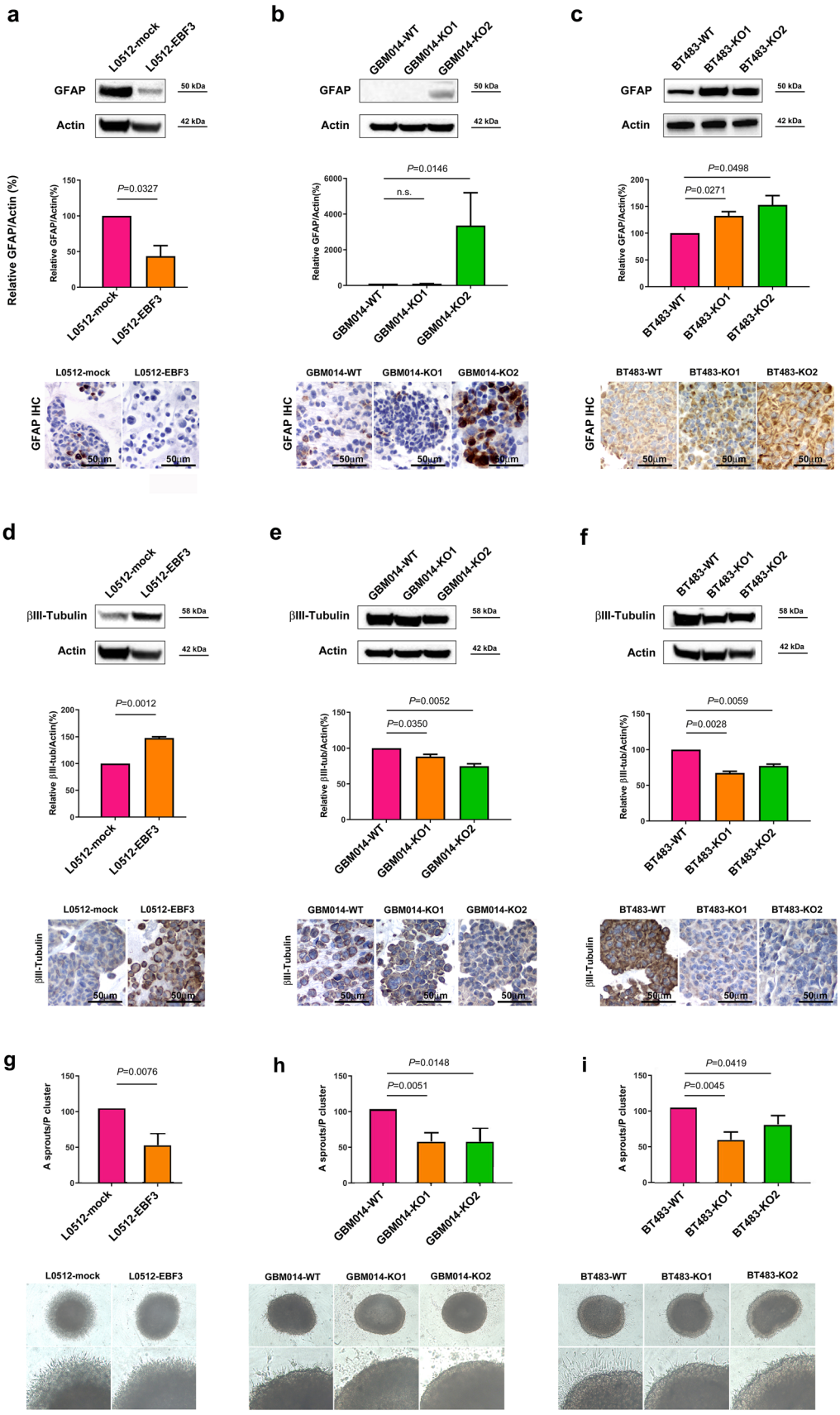
a
L0512-mock
L0512-EBF3
GFAP
Actin
50 kDa
42 kDa
Relative GFAP/Actin (%)
Relative GFAP/Actin(%)
P=0.0327
L0512-mock
L0512-EBF3
GFAP IHC
50μm
b
GBM014-WT
GBM014-KO1
GBM014-KO2
P=0.0146
n.s.
c
BT483-WT
BT483-KO1
BT483-KO2
P=0.0498
P=0.0271
d
βIII-Tubulin
58 kDa
Relative βIII-tub/Actin(%)
P=0.0012
e
P=0.0052
P=0.0350
f
P=0.0059
P=0.0028
g
A sprouts/P cluster
P=0.0076
h
P=0.0148
P=0.0051
i
P=0.0419
P=0.0045

◂**Fig. 4** EBF3 expression hampers glial differentiation favouring an early neuronal specification in GSCs along with enhanced invasive behaviour. **a** Upper: representative Western Blot for GFAP in control and transduced L0512 GSCs. Central: densitometric analysis of GFAP Western Blot in control and transduced L0512 GSCs. Lower: representative IHC for GFAP on control and transduced L0512 cell blocks. **b** Upper: representative Western Blot for GFAP in control and knockout GBM014 GSCs. Central: densitometric analysis of GFAP Western Blot in control and knockout GBM014 clones. Lower: representative IHC for GFAP on control and knockout GBM014 cell blocks. **c** Upper: representative Western Blot for GFAP in control and knockout BT483 GSCs. Central: densitometric analysis of GFAP Western Blot in control and knockout BT483 clones. Lower: representative IHC for GFAP on control and knockout BT483 cell blocks. **d** Upper: representative Western Blot for βIII-tubulin in control and transduced L0512 GSCs. Central: densitometric analysis of βIII-tubulin Western Blot in control and transduced L0512 GSCs. Lower: representative IHC for βIII-tubulin on control and transduced L0512 cell blocks. **e** Upper: representative Western Blot for βIII-tubulin in control and knockout GBM014 GSCs. Central: densitometric analysis of βIII-tubulin Western Blot in control and knockout GBM014 clones. Lower: representative IHC for βIII-tubulin on control and knockout GBM014 cell blocks. **f** Upper: representative Western Blot for βIII-tubulin in control and knockout BT483 GSCs. Central: densitometric analysis of βIII-tubulin Western Blot in control and knockout BT483 clones. Lower: representative IHC for βIII-tubulin on control and knockout BT483 cell blocks. Error bar represents mean ± s.d. of $n = 3$ independent experiments, two-tailed, unpaired Student's *t*-test. **g** Upper: quantification of control and EBF3 transduced L0512 tumour spheroid invasion. Lower: representative images of L0512 tumour spheroid invasion are shown. **h** Upper: quantification of control and knockout GBM014 tumour spheroid invasion. Lower: representative images of GBM014 tumour spheroid invasion are shown. **i** Upper: quantification of control and knockout BT483 tumour spheroid invasion. Lower: representative images of BT483 tumour spheroid invasion are shown

blocks (Fig. 4b and c). On the contrary, βIII-tubulin resulted higher in all the EBF3-expressing GSCs (GBM014-WT, BT483-WT, L0512-EBF3) as compared to the EBF3-negative counterparts (Fig. 4d–f). Of note, the heterozygous GBM014-KO1 showed a barely detectable GFAP expression and the same βIII-tubulin levels as compared to the GBM014-WT, suggesting that the residual functional EBF3 allele was sufficient to hamper glial differentiation (Fig. 4b and 4e central lanes). As described, GBM-PNC are highly infiltrating tumours with significant increased propensity for cerebrospinal dissemination and extra-CNS metastasis. We thus assessed the invasive capacity of the transduced clones by the invasion assay. Of note, EBF3-positive GBM014-WT and BT483-WT clones showed a significantly higher invasive capacity when compared to the respective EBF3-knockout clones (GBM014-KO1, GBM014-KO2, BT483-KO1, BT483-KO2) (Fig. 4h–i). Surprisingly, the EBF3-transduced L0512-EBF3 showed a lower invasive capacity as compared to the EBF3 negative control L0512-mock (Fig. 4g). These data suggest that EBF3 may play a dual role promoting invasiveness in GBM-PNC while exerting a suppressive function in conventional GBM. To further investigate the impact of EBF3 expression on the GBM-PNC phenotype in a model better resembling human GBM, we generated GBM organoids from our GSCs clones. The EBF3-negative L0512-mock GSCs gave rise to organoids reminiscent of conventional GBMs with glial features, including atypical cells with eosinophilic cytoplasm and elongated hyperchromatic nuclei along, characterised by high levels of GFAP and low levels of βIII-tubulin expression. On the contrary, the EBF3-transduced L0512-EBF3 clone gave rise to organoids with a predominant PNC-like morphology composed of small to medium size cells with hyperchromatic nuclei, high N/C ratio and severe anaplasia with high levels of βIII-tubulin and low levels of GFAP expression (Fig. 5A). Accordingly, the EBF3-positive BT483-WT GSCs clones gave rise to organoids with a PNC-like morphology expressing high levels of βIII-tubulin, while GFAP was barely detected. Remarkably, BT483-KO1 and BT483-KO2 EBF3 knock-out clones acquired a glial morphology and immunophenotype with GFAP upregulation and βIII-tubulin downregulation similar to the L0512-mock clones (Fig. 5B). Intriguingly, the organoids derived from the GBM014-WT clones showed a biphasic morphology, being predominantly composed of anaplastic cells with PNC-like morphology and nuclear moulding along with clusters of cells with elongated nuclei and eosinophilic cytoplasm consistent with glial features (Fig. 5C). Interestingly, triple immunostains highlighted that PNC-areas, negative for GFAP and positive for βIII-tubulin expression, retained EBF3 expression, while clusters of cells with glial features, characterised by GFAP expression and lower levels of βIII-tubulin, downregulated EBF3 (Fig. 5C). As in the case of GBM014-WT, the organoid from heterozygous GBM014-KO1 showed a biphasic, although attenuated, aspect, with a higher prevalence of cells with a PNC-like morphology and few aggregates of cells with glial features, indicating that the residual functional EBF3 allele is sufficient to promote a biphasic phenotype. Immunophenotypic analysis showed overall lower levels of EBF3 expression, a few number of GFAP + aggregates and a diffuse, although faint, expression of βIII-tubulin. The GBM014-KO2 EBF3 knockout clone, featuring complete loss of EBF3 expression, gave rise to organoids with a prominent glial morphology with homogeneous and diffuse GFAP expression and low to negative expression of βIII-tubulin (Fig. 5C). These results suggest that GSCs forming GBM-PNC can modulate EBF3 expression during tumorigenesis producing a biphasic tumour with either glial or PNC-like morphology. In vitro data indicate that EBF3 expression hampers GSC glial differentiation, favouring a cell fate toward an early neuronal specification, albeit without reaching a mature state, as we have already reported in medulloblastoma [17] and as highlighted by the lack of mature neuronal markers, such as NeuN (not shown). Altogether, these data suggest that in the presence of EBF3 expression, GCSs preferentially

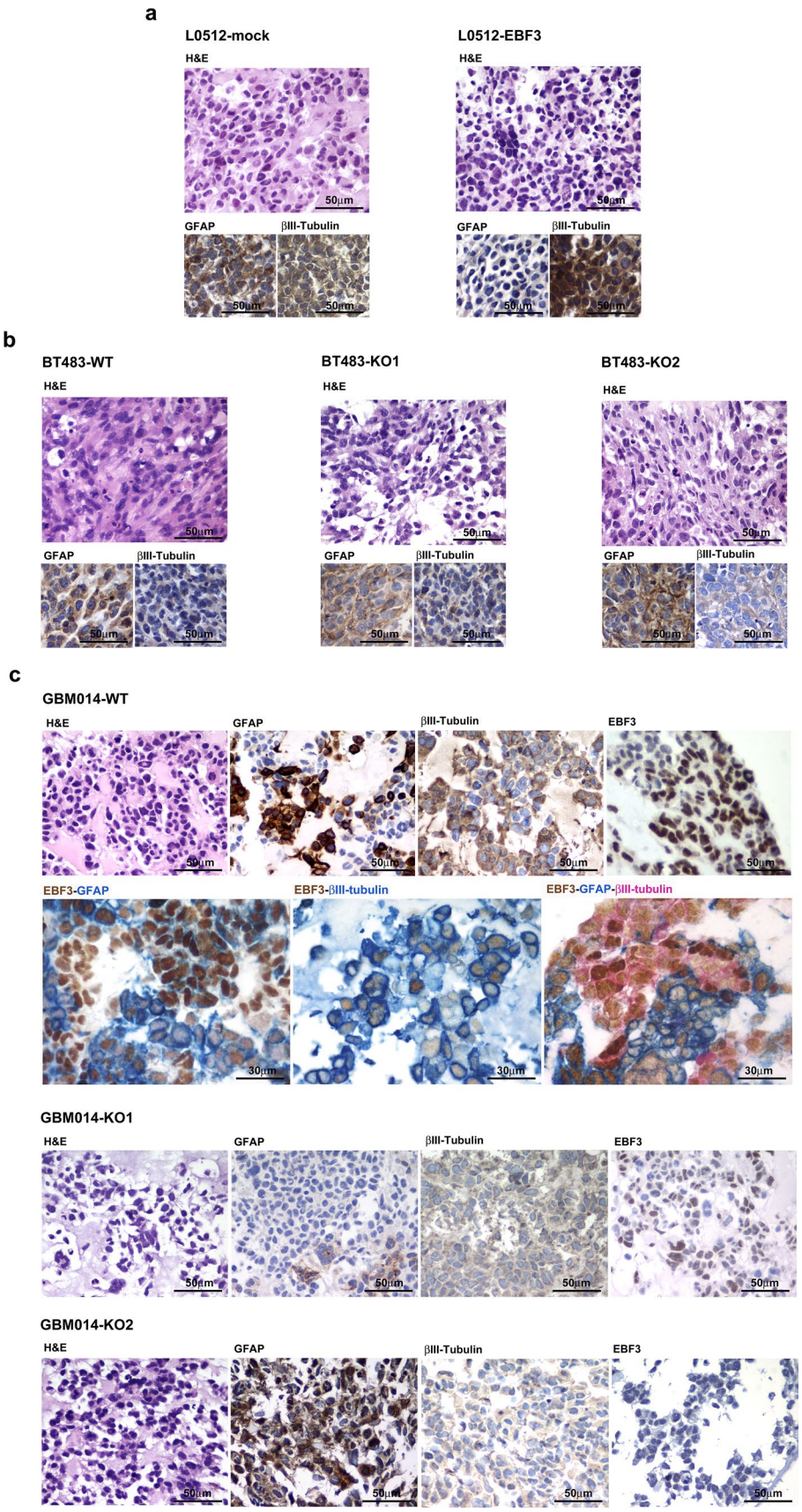

Fig. 5 EBF3 expression hampers glial differentiation favouring an early neuronal specification in glioblastoma organoids. **A** Upper: representative H&E images of the histology of L0512-mock (left) and L0512-EBF3 (right) organoids. Lower: representative IHC for GFAP (left) and βIII-tubulin (right) of L0512-mock and L0512-EBF3, respectively. **B** Upper: representative H&E images of the histology of BT483-WT (left), BT483-KO1 (central) and BT483-KO2 (right) organoids. Lower: representative IHC for GFAP (left) and βIII-tubulin (right) of BT483-WT, BT483-KO1 and BT483-KO2, respectively. **C** Upper: representative images of GBM014-WT organoids showing H&E staining, single IHC for EBF3, for GFAP, for βIII-tubulin and EBF3 IHC in double or triple staining with GFAP and βIII-tubulin. Central and lower strings show representative images of GBM014-KO1 and KO2 organoids stained with H&E, or IHC for EBF3, for GFAP and for βIII-tubulin

show an early neuronal rather than a glial phenotype, which is acquired in the absence of EBF3 expression. Finally, we investigated in our organoid cultures if loss or gain of EBF3 expression impacts on the proliferative properties of tumour cells. However, we did not found any significant difference in the proliferation assays between GBM WT, EBF3 KO and EBF3 transduced clones, suggesting that EBF3 is related to the cell fate and invasiveness rather than proliferation.

The PNC phenotype relies on the expression of EBF3 which is directly controlled by MYC transcription factors in accessible chromatin sites

Given the contribution of EBF3 in defining the PNC component in GBM-PNC, we next investigated the possible mechanisms involved in regulating the expression of EBF3. After selecting transcription factors whose transcripts are enriched in the PNC component (Supplementary Fig. 6A and Supplementary Table 8), we predicted the transcription factor DNA binding motifs enriched at the *cis*-regulatory elements (CREs) of *EBF3* (Supplementary Fig. 6B and Supplementary Tables 9 and 10). We identified the MYC family members as promising candidates, as their binding motifs resided within the promoter and the putative enhancers of *EBF3* (Fig. 6a). The potential role of MYC and MYCN as EBF3 regulator in the PNC component of GBM-PNC was further corroborated by immunohistochemical analysis, showing that the expression of either MYC or MYCN is mainly confined to the PNC component in a mutually exclusive fashion within the same tumour (Fig. 6b and c and Supplementary Table 4). To investigate whether MYC transcription factors modulated the differential expression of EBF3, we first characterised the chromatin state of the five putative CREs of *EBF3* by ChIP assays. We measured an increased deposition of the active mark H3K27ac on all the CREs, in the EBF3 + GSCs (Fig. 6d). In the same setting, we found that MYC occupancy was higher at the promoter and upstream enhancers of EBF3 + GSCs. Of note, EBF3-GSCs showed the unique binding of MYCN at all the CREs (Fig. 6e, Supplementary Fig. 6C and D), thus indicating an uncoupling between the MYCN occupancy and transcription activation. We reasoned that the differences in EBF3 expression might be related to other epigenetic changes, such as DNA methylation. Indeed, patient DNA methylation profiling highlighted a lower methylation level at the CREs of the EBF3 locus, among the PNC components of GBM (Supplementary Fig. 6E). This pattern was further confirmed by analysing the DNA methylation level at the EBF3 promoter among GSCs samples (Fig. 6f), indicating that the low expression level of the gene was strictly associated with the DNA methylation state. These results suggest that MYC and MYCN binding to the CREs depend on their chromatin state, with MYC positively regulating EBF3 expression in a pre-existing active chromatin environment.

Discussion

GBM-PNC is a rare histological variant of GBM, frequently acknowledged as conventional GBM, but recently recognized as a separate entity based on methylation profiling [80]. The biphasic nature of GBM-PNC provides a unique tool to investigate tumour heterogeneity and the relationships between genetic alterations, tumour biology, and their phenotypic manifestations. Here, we extensively characterised a consistent cohort of GBM-PNC by using integrated histopathological, genetic and transcriptomic analysis. Our data indicate that in GBM-PNC both components are highly enriched in genetic alterations that directly disrupt cell cycle regulation (*RB* inactivation or *CDK4* amplification) and inactivate the p53 pathway (*TP53* mutations or *MDM2/4* amplification). However, the PNC component displays additional upregulation of transcriptional pathways associated with proliferative activity, including overexpression of MYC target genes. Furthermore, enrichment in the Cahoy neuronal signature in the PNC component is consistent with a "neural progenitor cell phenotype", as supported by immunohistochemical profiling and the enrichment of RB1 pathway downregulated genes as well as MYC and E2F targets genes. These observations align with our previous findings indicating that GBMs comprise functionally distinct GSC subclones, each characterized by a unique transcriptional profile, regardless of a common genetic background [21]. Notably, we have also shown a strong correlation between malignant potential and GSC subclones displaying a 'neural progenitor cell' (NPC-like) transcriptional profile, according with recent single-cell categorizations of GBM cellular states [56]. These data support the notion that the PNC component in GBM arises preferentially through the selection of distinctive transcriptional programs that retain cells in a more undifferentiated primitive neuronal state contributing to the PNC phenotype and tumour progression. Remarkably, the PNC component shows a selective and robust mutually exclusive overexpression of MYC and MYCN transcription factors. These factors regulate a variety of biological processes including growth, proliferation, differentiation and apoptosis [20]. Overexpression of the MYC family genes, whether through amplification or loss of negative transcriptional control, has been implicated in tumorigenesis across various types of tumours [5, 13, 29, 55]. Of note, sustained MYC overexpression combined with *TP53* and *RB1*-deletion is frequently observed in tumours of neuroendocrine cell lineage [7, 43, 53]. It has been reported that loss-of-function alterations in *RB1* and *TP53* alongside high MYC expression generate in vivo lung cancers with 100% penetrance, often

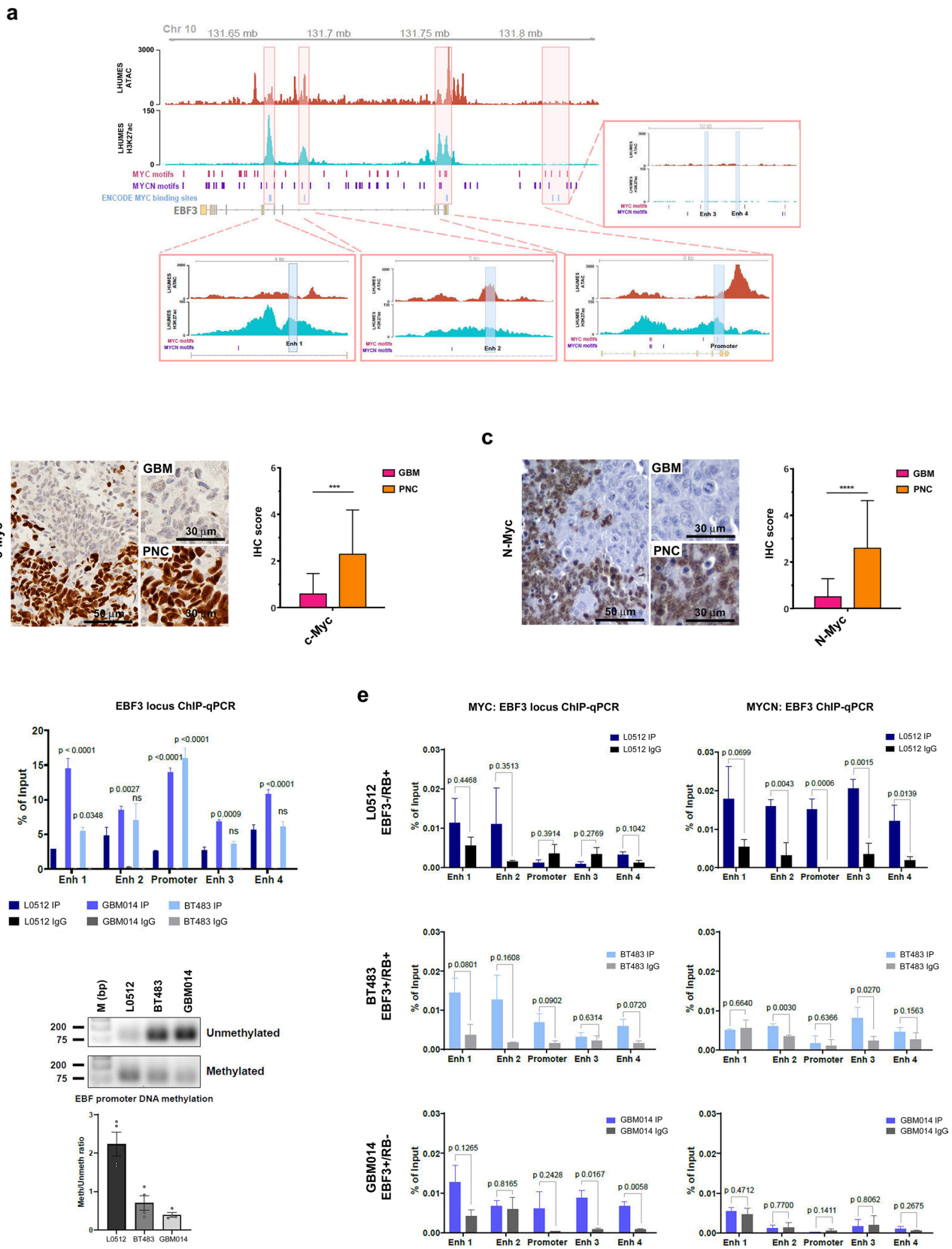
a
Chr 10
131.65 mb
131.7 mb
131.75 mb
131.8 mb
LHUMES ATAC
LHUMES H3K27ac
MYC motifs
MYCN motifs
ENCODE MYC binding sites
EBF3
Enh 1
Enh 2
Enh 3
Enh 4
Promoter
b
c-Myc
GBM
PNC
30 μm
50 μm
IHC score
***
c
N-Myc
****
d
EBF3 locus ChIP-qPCR
% of Input
L0512 IP
L0512 IgG
GBM014 IP
GBM014 IgG
BT483 IP
BT483 IgG
Enh 1
Enh 2
Promoter
Enh 3
Enh 4
e
MYC: EBF3 locus ChIP-qPCR
MYCN: EBF3 ChIP-qPCR
L0512 EBF3-/RB+
BT483 EBF3+/RB+
GBM014 EBF3+/RB-
f
M (bp)
L0512
BT483
GBM014
Unmethylated
Methylated
EBF promoter DNA methylation
Meth/Unmeth ratio

◂**Fig. 6** Role of cMYC and NMYC in shaping EBF3 chromatin state and modulating its expression in PNC and conventional GBM cell models. **a** Genomic view of EBF3 gene with ATAC-seq peaks (red track, GSE109706) and H3K27ac peaks (turquoise track, GSE125658) from public datasets, indicating accessible regions for transcription factor binding in LUHMES cell lines having high EBF3 expression. Below the tracks, the positions of high confidence predicted cMYC and NMYC binding motifs (p-value < 3e−6) are reported, as well as ENCODE ChIPseq-validated TFBSs in neuronal lineages. Pink highlights indicate zoom-ins of the regions that were selected as target cMYC and NMYC binding sites named as Binding site 2, Binding site 1, Promoter and Enhancer. In the zoom-in panels, light blue highlights indicate the regions of ENCODE validated TFBSs within which the primers used in ChIP-qPCR were designed. **b** IHC for cMyc and NMyc **c** of representative GBM-PNC tumours (right panels shows higher magnification of cMyc and NMyc immunoreactivity within the GBM and PNC components, respectively); plot displays the evaluation and scoring for cMyc and NMyc IHC in the tumours of the entire study cohort ($n = 24$) determined according to criteria stated in the Material and Methods section. Error bar represents mean ± s.d., two-tailed, unpaired Student's t-test. **d** ChIP-qPCR for H3K27ac histone modification on the regions highlighted in panel c. qPCR values were reported as percentage of Input DNA. Signals for both cMYC/NMYC and IgG are reported. The plotted values are the mean ± S.E.M. of three independent biological replicates. Statistical significance was calculated for the GSCs GBM014 and BT483 with respect to the reference GBM GSCs L0512 using two-way ANOVA. **e** ChIP-qPCR for cMYC (left) and NMYC (right) on the selected binding sites of EBF3 gene locus in the analysed GSCs: L0512, BT483 AND GBM014 (from left to right). qPCR values were reported as percentage of Input DNA. Signals for both cMYC/NMYC and IgG are reported. The plotted values are the mean ± S.E.M. of three independent biological replicates. Statistical significance was calculated for each target region for the IP with respect to the IgG signal using paired t-test. **f** Lower: Methylation specific primers PCR quantification of 4 biological replicates reported as relative bands intensity for the methylated over unmethylated PCR product for the three GSCc. Barplots report the mean ± S.E.M. Upper: representative agarose gel image of methylation specific primers PCR products. From left to right gel lanes are: DNA ladder 1kp plus, L0512, BT483 and GBM014

exhibiting heterogeneous patterns of neuroendocrine differentiation [13]. In addition, *MYCN* gene amplification is common in paediatric tumours originating from neuroectodermal progenitor cells, including CNS embryonal tumours, such as medulloblastoma, retinoblastoma and neuroblastoma [66]. Notably, MYC and MYCN overexpression, combined with *RB1* and/or *TP53* alterations, distinguishes a subset of aggressive tumours with a poor prognosis [69, 76], as also previously reported by our group in medulloblastoma [16], supporting that combinations of *RB1-MYC-TP53* molecular alterations contribute to enhance tumour aggressiveness. However, a small but unique subgroup of retinoblastomas have been identified with no detectable mutation in *RB1* gene, but with high levels of *MYCN* gene amplification [28, 68, 95], likely leading to RB1 down-regulation, supporting our observation that in the BT483 *RB1* wild-type GSC line *MYCN* amplification is sufficient to generate a tumour with a PNC-like features. How *MYC/MYCN* amplification and/or overexpression impacts on the cell fate determinant and tumour heterogeneity remains to be defined. Beyond gene amplification, MYC overexpression is also regulated epigenetically [29]. Recent studies suggest that modulation of MYC expression drives functional transcriptional heterogeneity in cancer cells in response to stressful events [46]. These unique spatial and temporal transcriptional states heavily impact on tumour cell biology and phenotype. Our data indicate that the concomitant presence of genetic alterations affecting both cell cycle and *TP53* pathway control, strongly predispose GBMs to develop a concomitant poorly differentiated primitive phenotype, driven by *MYC*-mediated EBF3 transcription in a subset of GSCs. We show that the PNC phenotype relies on expression of EBF3, an early neurogenic transcription factor, which is directly controlled by MYC transcription factors in accessible chromatin sites. In line with these observations, we found EBF3 consistently and selectively expressed in the PNC component of GBM-PNCs, along with a clonal skew toward a neuronal signature and expression of early neuronal markers, such as βIII-Tubulin and Synaptophysin. EBF3 is a DNA-binding transcriptional factor with an important role in neuronal differentiation and regional specification during neurogenesis [25, 31]. Its expression is restricted to early post-mitotic progenitor cells committed to the neuronal phenotype [30], as also shown in human organoids where *EBF3* has been found among the top upregulated genes at earlier time points during neuronal differentiation [72]. Accordingly, our data show that in immature teratoma, a recognized human model of neurogenesis in vivo, EBF3 is selectively expressed in maturing neuroblasts. As expected, in GBM-PNC EBF3 is selectively expressed in the PNC component, along with the expression of early neuronal markers, such as βIII-tubulin and synaptophysin. In vitro studies support the evidence that EBF3 has a pivotal role in hampering glial differentiation and promoting an early neuronal phenotype, typical of the PNC component. A variety of reports have shown that EBF3 may also exert oncogenic functions, depending on the tumour type, and epigenetic modifications at the *EBF3* promoter have been reported to be associated with tumour aggressiveness and progression in different cancers [67]. We have previously reported that elevated expression of EBF3 in medulloblastoma is associated with enhanced tumorigenesis [17]. In melanoma, hypermethylation of the *EBF3* promoter increases its expression and induces cell proliferation, migration and invasion [12], and upregulation of EBF3 in nasopharyngeal carcinoma promotes tumour invasiveness and drives cancer metastasis [23]. Thus, EBF3 expression in the PNC component may also exert a key role in mediating the proliferation and the invasive behaviour, as we demonstrated in the GBM-PNC derived GSCs and organoids, according to the fact that GBM-PNC are highly infiltrating tumours with a significantly propensity for CSF

dissemination and extra-CNS metastasis. On the other hand, in GSCs derived from conventional GBMs, EBF3 inhibits the invasive behaviour, in line with data suggesting a potential role as tumour suppressor, as it is inactivated by methylation or deletion in up to 90% of GBMs [93]. As such, our data indicate that in GSCs derived from GBM-PNC the *EBF3* locus is accessible by mean of H3K27 histone acetylation, while it is not accessible for transcription in GSCs derived from conventional GBMs. These observations, along with the transcriptional profiling of the tumours, suggest a different epigenetic setting and different transcriptional regulation mechanisms between the GBM and PNC components of GBM-PNC, despite the same genetic background. Indeed, *RB1* alterations, a recognized hallmark of GBM-PNC, along with other early driver alterations, including *TP53* and *IDH* mutations, are shared between the two components. Interestingly, *RB1* alterations have been also associated with tumour instability, hypermutated gene signature, aberrant cell cycle and defects in mismatch repair (MMR) genes [47, 64, 79]. In addition, *RB1* has been shown to be commonly inactivated after receiving both chemo- and radiotherapy, providing further insight into the contribution of genetic alterations in cell cycle and DNA repair-related genes to tumour evolution and progression [64]. We hypothesised that the phenotypical skewing between the GBM and PNC components may be associated to *RB1*-related genetic instability that may be considered as a predisposing alteration for GBM-PNC determination. Our data support the evidence that *RB1* pathway alterations, including CDK4 and E2F upregulation, may contribute to tumour instability with the emergence, within a GBM background, of a subpopulation of undifferentiated neuroectodermal progenitors leading to the expansion of the PNC component through the *RB1-MYC-EBF3* axis activation in a pre-existing active chromatin state. This evidence, along with a deeper understanding of the dynamics that generate tumour heterogeneity in HGGs, will have significant implications for the development of novel therapies. To date, although GBM-PNCs represent a unique histological subtype, the therapeutic schedule adopted is substantially the same as for conventional GBMs. However, when recognized, and due to the high risk of CSF dissemination, an association with platinum-based chemotherapy has been proposed. Despite these aggressive therapeutic schedules, GBM-PNC becomes rapidly chemo-resistant highlighting the urgent need for novel therapeutic approaches. It has been reported that Aurora kinase inhibition, in association to first-line chemotherapy, is a potential valuable therapeutic approach for MYC-driven neuroendocrine lung cancers, which significantly improves chemotherapy response and extends survival [32]. In this context, EBF3 expression may serve as a valuable biomarker for GBM-PNC patient stratification that may benefit for an associated MYC targeted treatment approach.

Supplementary Information The online version contains supplementary material available at https://doi.org/10.1007/s00401-025-02845-y.

Acknowledgements We thank Wilma Pellegrini, Daniela Medicina and Mattia Bugatti for technical support and colleagues of the Neuro-Oncology Group from Spedali Civili of Brescia. A special thanks goes to Prof. Piero Dalerba for his suggestions and helpful critical discussions.

Author contributions Conceptualization and methodology: P.L.P., F.P., C.B. and A.Z. Formal analysis and investigation: F.P., F.O., S.L., F.D.B., E.S., M.G., P.B., G.C., M.C. and D.C.; Data analysis support and revision: C.I., P.B., M.P. and D.M. Writing and original draft preparation: P.L.P., F.P., C.B. Writing, reviewing and editing: P.L.P., F.P., C.B., P.M., R.R., R.G., A.Z. Clinical samples and clinical data: P.L.P., F.P. and M.C. Funding acquisition: P.L.P. and C.B. All authors contributed to data analysis/interpretation and approved the final version of this manuscript. The first draft of the manuscript was written by P.L.P. and F.P. All authors commented on previous versions of the manuscript and approved the final version.

Funding This work was supported by (Grant RF-2016-02361014) and "Associazione dedicato A te" to PLP, AIRC—Italian Association for Cancer Research Investigator Grant N. 28836 to C.B.; RC 2022–2024, Ministero della Salute to C.B., and Comitato per Albi98 to C.B.; PRIN2020 cod. 20205TF444 and PRIN2022 cod. 20224NCSN5 to P.M. and PNRR MNESYS—A multiscale integrated approach to the study of the nervous system in health and disease to P.M.

Data availability RNA seq and NGS analysis are summarised in Supplementary Tables. Raw data are available at the European Nucleotide Archive under project accession number PRJEB59891, study ERP144936 (https://www.ebi.ac.uk/ena/browser/search). All other data supporting the findings of this study are available within the article and its Supplementary Information.

Declarations

Conflict of interest The authors declare that there are no competing interests.

Ethics approval and consent to participate All methods and experimental protocols related to human subjects were approved and carried out in compliance with the Declaration of Helsinki and with policies approved by the Institutional Review Board of Ethics Committee of Spedali Civili of Brescia. Surgical cases of human gliomas were part of the archival material obtained for diagnostic purposes from the Pathology Unit at Spedali Civili of Brescia, University of Brescia. Specifically, for retrospective and exclusively observational studies on archival material obtained for diagnostic purposes, patient consent was not needed (Delibera del Garante n. 52 del 24/7/2008 and DL 193/2003).

Consent for publication Not applicable.

References

1. Alexander BM, Cloughesy TF (2017) Adult glioblastoma. J Clin Oncol 35:2402–2409. https://doi.org/10.1200/jco.2017.73.0119
2. Ambrogini P, Lattanzi D, Ciuffoli S, Agostini D, Bertini L, Stocchi V et al (2004) Morpho-functional characterization of neuronal cells at different stages of maturation in granule cell layer

of adult rat dentate gyrus. Brain Res 1017:21–31. https://doi.org/10.1016/j.brainres.2004.05.039
3. Antonelli M, Poliani PL (2022) Adult type diffuse gliomas in the new 2021 WHO classification. Pathologica 114:397–409. https://doi.org/10.32074/1591-951X-823
4. Bernal A, Arranz L (2018) Nestin-expressing progenitor cells: function, identity and therapeutic implications. Cell Mol Life Sci 75:2177–2195. https://doi.org/10.1007/s00018-018-2794-z
5. Beroukhim R, Mermel CH, Porter D, Wei G, Raychaudhuri S, Donovan J et al (2010) The landscape of somatic copy-number alteration across human cancers. Nature 463:899–905. https://doi.org/10.1038/nature08822
6. Bhaduri A, Di Lullo E, Jung D, Muller S, Crouch EE, Espinosa CS et al (2020) Outer radial glia-like cancer stem cells contribute to heterogeneity of glioblastoma. Cell Stem Cell 26(48–63):e46. https://doi.org/10.1016/j.stem.2019.11.015
7. Bragelmann J, Bohm S, Guthrie MR, Mollaoglu G, Oliver TG, Sos ML (2017) Family matters: how MYC family oncogenes impact small cell lung cancer. Cell Cycle 16:1489–1498. https://doi.org/10.1080/15384101.2017.1339849
8. Cahoy JD, Emery B, Kaushal A, Foo LC, Zamanian JL, Christopherson KS et al (2008) A transcriptome database for astrocytes, neurons, and oligodendrocytes: a new resource for understanding brain development and function. J Neurosci 28:264–278. https://doi.org/10.1523/jneurosci.4178-07.2008
9. Capper D, Jones DTW, Sill M, Hovestadt V, Schrimpf D, Sturm D et al (2018) DNA methylation-based classification of central nervous system tumours. Nature 555:469–474. https://doi.org/10.1038/nature26000
10. Capper D, Stichel D, Sahm F, Jones DTW, Schrimpf D, Sill M et al (2018) Practical implementation of DNA methylation and copy-number-based CNS tumor diagnostics: the Heidelberg experience. Acta Neuropathol 136:181–210. https://doi.org/10.1007/s00401-018-1879-y
11. Cerami E, Gao J, Dogrusoz U, Gross BE, Sumer SO, Aksoy BA et al (2012) The cBio cancer genomics portal: an open platform for exploring multidimensional cancer genomics data. Cancer Discov 2:401–404. https://doi.org/10.1158/2159-8290.CD-12-0095
12. Chatterjee A, Stockwell PA, Ahn A, Rodger EJ, Leichter AL, Eccles MR (2017) Genome-wide methylation sequencing of paired primary and metastatic cell lines identifies common DNA methylation changes and a role for EBF3 as a candidate epigenetic driver of melanoma metastasis. Oncotarget 8:6085–6101. https://doi.org/10.18632/oncotarget.14042
13. Chen J, Guanizo A, Luong Q, Jayasekara WSN, Jayasinghe D, Inampudi C et al (2022) Lineage-restricted neoplasia driven by Myc defaults to small cell lung cancer when combined with loss of p53 and Rb in the airway epithelium. Oncogene 41:138–145. https://doi.org/10.1038/s41388-021-02070-3
14. Chkheidze R, Raisanen J, Gagan J, Richardson TE, Pinho MC, Raj K et al (2021) Alterations in the RB pathway with inactivation of RB1 characterize glioblastomas with a primitive neuronal component. J Neuropathol Exp Neurol 80:1092–1098. https://doi.org/10.1093/jnen/nlab109
15. Cominelli M, Grisanti S, Mazzoleni S, Branca C, Buttolo L, Furlan D et al (2015) EGFR amplified and overexpressing glioblastomas and association with better response to adjuvant metronomic temozolomide. J Natl Cancer Inst 107(5):djv041. https://doi.org/10.1093/jnci/djv041
16. Conti V, Cominelli M, Pieri V, Gallotti AL, Pagano I, Zanella M et al (2021) mTORC1 promotes malignant large cell/anaplastic histology and is a targetable vulnerability in SHH-TP53 mutant medulloblastoma. JCI Insight 6(23):e153462. https://doi.org/10.1172/jci.insight.153462
17. Corno D, Pala M, Cominelli M, Cipelletti B, Leto K, Croci L et al (2012) Gene signatures associated with mouse postnatal hindbrain neural stem cells and medulloblastoma cancer stem cells identify novel molecular mediators and predict human medulloblastoma molecular classification. Cancer Discov 2(6):554–568. https://doi.org/10.1158/2159-8290.cd-11-0199
18. Corti G, Bartolini A, Crisafulli G, Novara L, Rospo G, Montone M et al (2019) A genomic analysis workflow for colorectal cancer precision oncology. Clin Colorectal Cancer 18:91-101.e103. https://doi.org/10.1016/j.clcc.2019.02.008
19. Crisafulli G, Mussolin B, Cassingena A, Montone M, Bartolini A, Barault L et al (2019) Whole exome sequencing analysis of urine trans-renal tumour DNA in metastatic colorectal cancer patients. ESMO Open 4(6):e000572. https://doi.org/10.1136/esmoopen-2019-000572
20. Dang CV (2012) MYC on the path to cancer. Cell 149:22–35. https://doi.org/10.1016/j.cell.2012.03.003
21. De Bacco F, Orzan F, Crisafulli G, Prelli M, Isella C, Casanova E et al (2023) Coexisting cancer stem cells with heterogeneous gene amplifications, transcriptional profiles, and malignancy are isolated from single glioblastomas. Cell Rep 42(8):112816. https://doi.org/10.1016/j.celrep.2023.112816
22. De Bacco F, Orzan F, Erriquez J, Casanova E, Barault L, Albano R et al (2021) ERBB3 overexpression due to miR-205 inactivation confers sensitivity to FGF, metabolic activation, and liability to ERBB3 targeting in glioblastoma. Cell Rep 36(4):109455. https://doi.org/10.1016/j.celrep.2021.109455
23. Ding S, Wang X, Lv D, Tao Y, Liu S, Chen C et al (2022) EBF3 reactivation by inhibiting the EGR1/EZH2/HDAC9 complex promotes metastasis via transcriptionally enhancing vimentin in nasopharyngeal carcinoma. Cancer Lett 527:49–65. https://doi.org/10.1016/j.canlet.2021.12.010
24. Dobin A, Davis CA, Schlesinger F, Drenkow J, Zaleski C, Jha S et al (2013) STAR: ultrafast universal RNA-seq aligner. Bioinformatics 29:15–21. https://doi.org/10.1093/bioinformatics/bts635
25. Dubois L, Bally-Cuif L, Crozatier M, Moreau J, Paquereau L, Vincent A (1998) XCoe2, a transcription factor of the Col/Olf-1/EBF family involved in the specification of primary neurons in Xenopus. Curr Biol 8(4):199–209. https://doi.org/10.1016/s0960-9822(98)70084-3
26. Dulai MS, Bosanko CM, Wang AM, Horoupian DS, Boodin S, Chen PY et al (2004) Mixed cystic gliosarcoma and primitive neuroectodermal tumor: a case report. Clin Neuropathol 23:218–222 (**PMID: 15581024**)
27. Erickson LA, Lloyd RV (2004) Practical markers used in the diagnosis of endocrine tumors. Adv Anat Pathol 11:175–189. https://doi.org/10.1097/01.pap.0000131824.77317.a7
28. Ewens KG, Bhatti TR, Moran KA, Richards-Yutz J, Shields CL, Eagle RC et al (2017) Phosphorylation of pRb: mechanism for RB pathway inactivation in MYCN-amplified retinoblastoma. Cancer Med 6:619–630. https://doi.org/10.1002/cam4.1010
29. Gabay M, Li Y, Felsher DW (2014) MYC activation is a hallmark of cancer initiation and maintenance. Cold Spring Harbor Perspect Med 4(6):a014241. https://doi.org/10.1101/cshperspect.a014241
30. Garcia-Dominguez M, Poquet C, Garel S, Charnay P (2003) Ebf gene function is required for coupling neuronal differentiation and cell cycle exit. Development 130:6013–6025. https://doi.org/10.1242/dev.00840
31. Garel S, Marin F, Mattei MG, Vesque C, Vincent A, Charnay P (1997) Family of Ebf/Olf-1-related genes potentially involved in neuronal differentiation and regional specification in the central nervous system. Dev Dyn 210(3):191–205. https://doi.org/10.1002/(SICI)1097-0177(199711)210:3%3c191::AID-AJA1%3e3.0.CO;2-B
32. Grunblatt E, Wu N, Zhang H, Liu X, Norton JP, Ohol Y et al (2020) MYCN drives chemoresistance in small cell lung cancer while USP7 inhibition can restore chemosensitivity. Genes Dev 34:1210–1226. https://doi.org/10.1101/gad.340133.120

33. Hubert CG, Rivera M, Spangler LC, Wu Q, Mack SC, Prager BC et al (2016) A three-dimensional organoid culture system derived from human glioblastomas recapitulates the hypoxic gradients and cancer stem cell heterogeneity of tumors found in vivo. Cancer Res 76:2465–2477. https://doi.org/10.1158/0008-5472.CAN-15-2402
34. Idilli AI, Pagani F, Kerschbamer E, Berardinelli F, Bernabé M, Cayuela ML et al (2020) Changes in the expression of pre-replicative complex genes in hTERT and ALT pediatric brain tumors. Cancers (Basel) 12(4):1028. https://doi.org/10.3390/cancers12041028
35. Ishizawa K, Kan-nuki S, Kumagai H, Komori T, Hirose T (2002) Lipomatous primitive neuroectodermal tumor with a glioblastoma component: a case report. Acta Neuropathol 103(2):193–198. https://doi.org/10.1007/s004010100436
36. Joseph NM, Phillips J, Dahiya S, Felicella M, Tihan T, Brat DJ et al (2013) Diagnostic implications of IDH1-R132H and OLIG2 expression patterns in rare and challenging glioblastoma variants. Mod Pathol 26:315–326. https://doi.org/10.1038/modpathol.2012.173
37. Kaplan KJ, Perry A (2007) Gliosarcoma with primitive neuroectodermal differentiation: case report and review of the literature. J Neurooncol 83:313–318. https://doi.org/10.1007/s11060-007-9331-5
38. Kempermann G, Jessberger S, Steiner B, Kronenberg G (2004) Milestones of neuronal development in the adult hippocampus. Trends Neurosci 27:447–452. https://doi.org/10.1016/j.tins.2004.05.013
39. Kim J, Min SY, Lee HE, Kim WH (2012) Aberrant DNA methylation and tumor suppressive activity of the EBF3 gene in gastric carcinoma. Int J Cancer 130:817–826. https://doi.org/10.1002/ijc.26038
40. Korshunov A, Capper D, Reuss D, Schrimpf D, Ryzhova M, Hovestadt V et al (2016) Histologically distinct neuroepithelial tumors with histone 3 G34 mutation are molecularly similar and comprise a single nosologic entity. Acta Neuropathol 131:137–146. https://doi.org/10.1007/s00401-015-1493-1
41. Lagace DC, Whitman MC, Noonan MA, Ables JL, DeCarolis NA, Arguello AA et al (2007) Dynamic contribution of nestin-expressing stem cells to adult neurogenesis. J Neurosci 27:12623–12629. https://doi.org/10.1523/JNEUROSCI.3812-07.2007
42. Lambert SA, Jolma A, Campitelli LF, Das PK, Yin Y, Albu M et al (2018) The human transcription factors. Cell 172:650–665. https://doi.org/10.1016/j.cell.2018.01.029
43. Lee JK, Phillips JW, Smith BA, Park JW, Stoyanova T, McCaffrey EF et al (2016) N-Myc drives neuroendocrine prostate cancer initiated from human prostate epithelial cells. Cancer Cell 29:536–547. https://doi.org/10.1016/j.ccell.2016.03.001
44. Liao Y, Smyth GK, Shi W (2014) featureCounts: an efficient general purpose program for assigning sequence reads to genomic features. Bioinformatics 30(7):923–930. https://doi.org/10.1093/bioinformatics/btt656
45. Liberzon A, Birger C, Thorvaldsdóttir H, Ghandi M, Mesirov JP, Tamayo P (2015) The molecular signatures database (MSigDB) hallmark gene set collection. Cell Syst 1:417–425. https://doi.org/10.1016/j.cels.2015.12.004
46. Liu C, Kudo T, Ye X, Gascoigne K (2023) Cell-to-cell variability in Myc dynamics drives transcriptional heterogeneity in cancer cells. Cell Rep 42:112401. https://doi.org/10.1016/j.celrep.2023.112401
47. Liu H, Tang X, Srivastava A, Pecot T, Daniel P, Hemmelgarn B et al (2015) Redeployment of Myc and E2f1-3 drives Rb-deficient cell cycles. Nat Cell Biol 17:1036–1048. https://doi.org/10.1038/ncb3210
48. Louis DN, Perry A, Wesseling P, Brat DJ, Cree IA, Figarella-Branger D et al (2021) The 2021 WHO classification of tumors of the central nervous system: a summary. Neuro Oncol 23:1231–1251. https://doi.org/10.1093/neuonc/noab106
49. Love MI, Huber W, Anders S (2014) Moderated estimation of fold change and dispersion for RNA-seq data with DESeq2. Genome Biol 15:550. https://doi.org/10.1186/s13059-014-0550-8
50. Lu HE, Yang YC, Chen SM, Su HL, Huang PC, Tsai MS et al (2013) Modelling neurogenesis impairment in down syndrome with induced pluripotent stem cells from trisomy 21 amniotic fluid cells. Exp Cell Res 319:498–505. https://doi.org/10.1016/j.yexcr.2012.09.017
51. Mazzoleni S, Galli R (2012) Gliomagenesis: a game played by few players or a team effort? Front Biosci 4:205–213. https://doi.org/10.2741/2370
52. Mazzoleni S, Politi LS, Pala M, Cominelli M, Franzin A, Sergi Sergi L et al (2010) Epidermal growth factor receptor expression identifies functionally and molecularly distinct tumor-initiating cells in human glioblastoma multiforme and is required for gliomagenesis. Cancer Res 70:7500–7513. https://doi.org/10.1158/0008-5472.CAN-10-2353
53. Mollaoglu G, Guthrie MR, Bohm S, Bragelmann J, Can I, Ballieu PM et al (2017) MYC drives progression of small cell lung cancer to a variant neuroendocrine subtype with vulnerability to aurora kinase inhibition. Cancer Cell 31:270–285. https://doi.org/10.1016/j.ccell.2016.12.005
54. Mootha VK, Lindgren CM, Eriksson KF, Subramanian A, Sihag S, Lehar J et al (2003) PGC-1alpha-responsive genes involved in oxidative phosphorylation are coordinately downregulated in human diabetes. Nat Genet 34:267–273. https://doi.org/10.1038/ng1180
55. Morton JP, Sansom OJ (2013) MYC-y mice: from tumour initiation to therapeutic targeting of endogenous MYC. Mol Oncol 7:248–258. https://doi.org/10.1016/j.molonc.2013.02.015
56. Neftel C, Laffy J, Filbin MG, Hara T, Shore ME, Rahme GJ et al (2019) An integrative model of cellular states, plasticity, and genetics for glioblastoma. Cell 178(835–849):e821. https://doi.org/10.1016/j.cell.2019.06.024
57. O'Leary B, Mandeville HC, Fersht N, Solda F, Mycroft J, Zacharoulis S et al (2016) Craniospinal irradiation with concomitant and adjuvant temozolomide–a feasibility assessment of toxicity in patients with glioblastoma with a PNET component. J Neurooncol 127:295–302. https://doi.org/10.1007/s11060-015-2033-5
58. Orzan F, Pagani F, Cominelli M, Triggiani L, Calza S, De Bacco F et al (2020) A simplified integrated molecular and immunohistochemistry-based algorithm allows high accuracy prediction of glioblastoma transcriptional subtypes. Lab Invest 13:020–0437. https://doi.org/10.1038/s41374-020-0437-0
59. Ostrom QT, Price M, Neff C, Cioffi G, Waite KA, Kruchko C et al (2023) CBTRUS statistical report: primary brain and other central nervous system tumors diagnosed in the United States in 2016–2020. Neuro Oncol 25:iv1–iv99. https://doi.org/10.1093/neuonc/noad149
60. Perry A, Miller CR, Gujrati M, Scheithauer BW, Zambrano SC, Jost SC et al (2009) Malignant gliomas with primitive neuroectodermal tumor-like components: a clinicopathologic and genetic study of 53 cases. Brain Pathol 19:81–90. https://doi.org/10.1111/j.1750-3639.2008.00167.x
61. Phi JH, Park SH, Paek SH, Kim SK, Lee YJ, Park CK et al (2007) Expression of Sox2 in mature and immature teratomas of central nervous system. Mod Pathol 20:742–748. https://doi.org/10.1038/modpathol.3800793
62. Pidsley R, Zotenko E, Peters TJ, Lawrence MG, Risbridger GP, Molloy P et al (2016) Critical evaluation of the Illumina MethylationEPIC BeadChip microarray for whole-genome DNA methylation profiling. Genome Biol 17:208. https://doi.org/10.1186/s13059-016-1066-1

63. Prelaj A, Rebuzzi SE, Caffarena G, Giron Berrios JR, Pecorari S, Fusto C et al (2018) Therapeutic approach in glioblastoma multiforme with primitive neuroectodermal tumor components: case report and review of the literature. Oncol Lett 15:6641–6647. https://doi.org/10.3892/ol.2018.8102
64. Rautajoki KJ, Jaatinen S, Hartewig A, Tiihonen AM, Annala M, Salonen I et al (2023) Genomic characterization of IDH-mutant astrocytoma progression to grade 4 in the treatment setting. Acta Neuropathol Commun 11:176. https://doi.org/10.1186/s40478-023-01669-9
65. Richards LM, Whitley OKN, MacLeod G, Cavalli FMG, Coutinho FJ, Jaramillo JE et al (2021) Gradient of developmental and injury response transcriptional states defines functional vulnerabilities underpinning glioblastoma heterogeneity. Nat Cancer 2:157–173. https://doi.org/10.1038/s43018-020-00154-9
66. Rindi G, Klimstra DS, Abedi-Ardekani B, Asa SL, Bosman FT, Brambilla E et al (2018) A common classification framework for neuroendocrine neoplasms: an international agency for research on cancer (IARC) and world health organization (WHO) expert consensus proposal. Mod Pathol 31:1770–1786. https://doi.org/10.1038/s41379-018-0110-y
67. Rodger EJ, Chatterjee A, Stockwell PA, Eccles MR (2019) Characterisation of DNA methylation changes in EBF3 and TBC1D16 associated with tumour progression and metastasis in multiple cancer types. Clin Epigenetics 11:114. https://doi.org/10.1186/s13148-019-0710-5
68. Rushlow DE, Mol BM, Kennett JY, Yee S, Pajovic S, Theriault BL et al (2013) Characterisation of retinoblastomas without RB1 mutations: genomic, gene expression, and clinical studies. Lancet Oncol 14:327–334. https://doi.org/10.1016/S1470-2045(13)70045-7
69. Schwermer M, Hiber M, Dreesmann S, Rieb A, Theissen J, Herold T et al (2019) Comprehensive characterization of RB1 mutant and MYCN amplified retinoblastoma cell lines. Exp Cell Res 375:92–99. https://doi.org/10.1016/j.yexcr.2018.12.018
70. Seki T, Namba T, Mochizuki H, Onodera M (2007) Clustering, migration, and neurite formation of neural precursor cells in the adult rat hippocampus. J Comp Neurol 502:275–290. https://doi.org/10.1002/cne.21301
71. Shalem O, Sanjana NE, Hartenian E, Shi X, Scott DA, Mikkelson T et al (2014) Genome-scale CRISPR-Cas9 knockout screening in human cells. Science 343:84–87. https://doi.org/10.1126/science.1247005
72. Smits LM, Magni S, Kinugawa K, Grzyb K, Luginbühl J, Sabate-Soler S et al (2020) Single-cell transcriptomics reveals multiple neuronal cell types in human midbrain-specific organoids. Cell Tissue Res 382:463–476. https://doi.org/10.1007/s00441-020-03249-y
73. Solomon DA, Wood MD, Tihan T, Bollen AW, Gupta N, Phillips JJ et al (2016) Diffuse midline gliomas with histone H3–K27M mutation: a series of 47 cases assessing the spectrum of morphologic variation and associated genetic alterations. Brain Pathol 26:569–580. https://doi.org/10.1111/bpa.12336
74. Song X, Andrew Allen R, Terence Dunn S, Fung KM, Farmer P, Gandhi S et al (2011) Glioblastoma with PNET-like components has a higher frequency of isocitrate dehydrogenase 1 (IDH1) mutation and likely a better prognosis than primary glioblastoma. Int J Clin Exp Pathol 4:651–660 (**PMID:22076165**)
75. Steinhaus R, Proft S, Schuelke M, Cooper DN, Schwarz JM, Seelow D (2021) MutationTaster2021. Nucleic Acids Res 49(W1):W446–W451. https://doi.org/10.1093/nar/gkab266
76. Strieder V, Lutz W (2003) E2F proteins regulate MYCN expression in neuroblastomas. J Biol Chem 278:2983–2989. https://doi.org/10.1074/jbc.M207596200
77. Stupp R, Hegi ME, Mason WP, van den Bent MJ, Taphoorn MJ, Janzer RC et al (2009) Effects of radiotherapy with concomitant and adjuvant temozolomide versus radiotherapy alone on survival in glioblastoma in a randomised phase III study: 5-year analysis of the EORTC-NCIC trial. Lancet Oncol 10:459–466. https://doi.org/10.1016/s1470-2045(09)70025-7
78. Subramanian A, Tamayo P, Mootha VK, Mukherjee S, Ebert BL, Gillette MA et al (2005) Gene set enrichment analysis: a knowledge-based approach for interpreting genome-wide expression profiles. Proc Natl Acad Sci U S A 102:15545–15550. https://doi.org/10.1073/pnas.0506580102
79. Suwala AK, Stichel D, Schrimpf D, Kloor M, Wefers AK, Reinhardt A et al (2021) Primary mismatch repair deficient IDH-mutant astrocytoma (PMMRDIA) is a distinct type with a poor prognosis. Acta Neuropathol 141:85–100. https://doi.org/10.1007/s00401-020-02243-6
80. Suwala AK, Stichel D, Schrimpf D, Maas SLN, Sill M, Dohmen H et al (2021) Glioblastomas with primitive neuronal component harbor a distinct methylation and copy-number profile with inactivation of TP53, PTEN, and RB1. Acta Neuropathol 142:179–189. https://doi.org/10.1007/s00401-021-02302-6
81. Szu JI, Tsigelny IF, Wojcinski A, Kesari S (2023) Biological functions of the Olig gene family in brain cancer and therapeutic targeting. Front Neurosci 17:1129434. https://doi.org/10.3389/fnins.2023.1129434
82. Takami H, Yoshida A, Fukushima S, Arita H, Matsushita Y, Nakamura T et al (2015) Revisiting TP53 mutations and immunohistochemistry–a comparative study in 157 diffuse gliomas. Brain Pathol 25:256–265. https://doi.org/10.1111/bpa.12173
83. Takayama Y, Matsumura N, Nobusawa S, Ikota H, Minegishi T, Yokoo H (2016) Immunophenotypic features of immaturity of neural elements in ovarian teratoma. Virchows Arch 468:337–343. https://doi.org/10.1007/s00428-015-1891-8
84. Tamai S, Kinoshita M, Sabit H, Furuta T, Miyashita K, Yoshimura K et al (2019) Case of metastatic glioblastoma with primitive neuronal component to the lung. Neuropathology 39:218–223. https://doi.org/10.1111/neup.12553
85. Tanner G, Barrow R, Ajaib S, Al-Jabri M, Ahmed N, Pollock S et al (2024) IDHwt glioblastomas can be stratified by their transcriptional response to standard treatment, with implications for targeted therapy. Genome Biol 25:45. https://doi.org/10.1186/s13059-024-03172-3
86. Verhaak RG, Hoadley KA, Purdom E, Wang V, Qi Y, Wilkerson MD et al (2010) Integrated genomic analysis identifies clinically relevant subtypes of glioblastoma characterized by abnormalities in PDGFRA, IDH1, EGFR, and NF1. Cancer Cell 17:98–110. https://doi.org/10.1016/j.ccr.2009.12.020
87. Walter DM, Venancio OS, Buza EL, Tobias JW, Deshpande C, Gudiel AA et al (2017) Systematic in vivo inactivation of chromatin regulating enzymes identifies Setd2 as a potent tumor suppressor in lung adenocarcinoma. Cancer Res 77:1719–1729. https://doi.org/10.1158/0008-5472.can-16-2159
88. Wang Q, Hu B, Hu X, Kim H, Squatrito M, Scarpace L et al (2017) Tumor evolution of glioma-intrinsic gene expression subtypes associates with immunological changes in the microenvironment. Cancer Cell 32(42–56):e46. https://doi.org/10.1016/j.ccell.2017.06.003
89. Wharton SB, Whittle IR, Collie DA, Bell HS, Ironside JW (2001) Gliosarcoma with areas of primitive neuroepithelial differentiation and extracranial metastasis. Clin Neuropathol 20(5):212–218 (**PMID: 11594506**)
90. Wheeler TC, Chin LS, Li Y, Roudabush FL, Li L (2002) Regulation of synaptophysin degradation by mammalian homologues of seven in absentia. J Biol Chem 277:10273–10282. https://doi.org/10.1074/jbc.M107857200
91. Willis JA, Overman MJ (2022) Inducing hypermutability to promote anti-PD-1 therapy response. Cancer Discov 12:1612–1614. https://doi.org/10.1158/2159-8290.CD-22-0492

92. Xu G, Zheng H, Li JY (2019) Next-generation whole exome sequencing of glioblastoma with a primitive neuronal component. Brain Tumor Pathol 36:129–134. https://doi.org/10.1007/s10014-019-00334-1
93. Zardo G, Tiirikainen MI, Hong C, Misra A, Feuerstein BG, Volik S et al (2002) Integrated genomic and epigenomic analyses pinpoint biallelic gene inactivation in tumors. Nat Genet 32:453–458. https://doi.org/10.1038/ng1007
94. Zhang J, Jiao J (2015) Molecular biomarkers for embryonic and adult neural stem cell and neurogenesis. Biomed Res Int 2015:727542. https://doi.org/10.1155/2015/727542
95. Zugbi S, Ganiewich D, Bhattacharyya A, Aschero R, Ottaviani D, Sampor C et al (2020) Clinical, genomic, and pharmacological study of MYCN-amplified RB1 wild-type metastatic retinoblastoma. Cancers (Basel) 12(9):2714. https://doi.org/10.3390/cancers12092714

Publisher's Note Springer Nature remains neutral with regard to jurisdictional claims in published maps and institutional affiliations.

Springer Nature or its licensor (e.g. a society or other partner) holds exclusive rights to this article under a publishing agreement with the author(s) or other rightsholder(s); author self-archiving of the accepted manuscript version of this article is solely governed by the terms of such publishing agreement and applicable law.

Authors and Affiliations

Francesca Pagani[1,2] · Francesca Orzan[3,4] · Sara Lago[5] · Francesca De Bacco[3,4] · Marta Prelli[3,4] · Manuela Cominelli[1] · Elena Somenza[1,6] · Magdalena Gryzik[1,7] · Piera Balzarini[1] · Davide Ceresa[8] · Daniela Marubbi[8,9] · Claudio Isella[3,4] · Giovanni Crisafulli[10] · Maura Poli[7] · Paolo Malatesta[8,9] · Rossella Galli[11] · Roberto Ronca[6] · Alessio Zippo[5] · Carla Boccaccio[3,4] · Pietro Luigi Poliani[1,12]

✉ Pietro Luigi Poliani
luigi.poliani@unibs.it

1 Pathology Unit, Department of Molecular and Translational Medicine, University of Brescia, Brescia, Italy

2 I Department of Medicine, University Medical Center Hamburg-Eppendorf, Hamburg, Germany

3 Candiolo Cancer Institute, FPO-IRCCS, Candiolo, 10060 Turin, Italy

4 Department of Oncology, University of Turin Medical School, Candiolo, 10060 Turin, Italy

5 Laboratory for Chromatin Biology and Epigenetics, CIBIO—Department of Cellular, Computational and Integrative Biology, University of Trento, Trento, Italy

6 Experimental Oncology and Immunology Unit, Department of Molecular and Translational Medicine, University of Brescia, Brescia, Italy

7 Biochemistry Unit, Department of Molecular and Translational Medicine, University of Brescia, Brescia, Italy

8 IRCCS Ospedale Policlinico San Martino, Genoa, Italy

9 Department of Experimental Medicine (DIMES), University of Genova, Genoa, Italy

10 IFOM ETS—The AIRC Institute of Molecular Oncology, 20139 Milan, Italy

11 Neural Stem Cell Biology Unit, Division of Neuroscience, IRCCS San Raffaele Hospital, Milan, Italy

12 Pathology Unit, IRCCS Ospedale San Raffaele, Milan, Italy